Research Square

Preprints are preliminary reports that have not undergone peer review.
They should not be considered conclusive, used to inform clinical practice,
or referenced by the media as validated information.

GMP-manufactured cell-free iPSC-derived bioactive preparation, iPSC Factor, promotes hyaluronic acid synthesis and extracellular matrix remodeling

Ren Shimamoto
I Peace, Ltd.
Kenta Sutou
I Peace, Ltd.
Ryo Motosugi
I Peace, Ltd.
Emi Tomoda
I Peace, Inc.
Sakura Tamaki
I Peace, Ltd.
Kazuhiko Kaji
Kose Co., Ltd.
Koji Tanabe
tanabe@ipeaceinc.com

I Peace, Inc.

Article

Keywords: iPSC Factor (iPSF), induced pluripotent stem cells (iPSCs), Hyaluronic acid (HA), Extracellular matrix (ECM) remodeling, GMP manufacturing, Skin regeneration / skin aging

Posted Date: November 25th, 2026

DOI: https://doi.org/10.21203/rs.3.rs-11374997/v1

License: This work is licensed under a Creative Commons Attribution 4.0 International License.
Read Full License

Additional Declarations: Competing interest reported. R.S., K.S., R.M., E.T., S.T., and K.T. are employees of I Peace, Inc. or I Peace, Ltd., which develops and sells iPSC Factor (iPSF), the product investigated in this

study. K.K. is an employee of KOSÉ Corporation.

GMP-manufactured cell-free iPSC-derived bioactive preparation, iPSC Factor, promotes hyaluronic acid synthesis and extracellular matrix remodeling

Ren Shimamoto[1], Kenta Sutou[1], Ryo Motosugi[1], Emi Tomoda[2], Sakura Tamaki[1], Kazuhiko Kaji[5] and Koji Tanabe[1,2,3,4*]

1. I Peace, Ltd., Kyodai Katsura Venture Plaza North 311, 1-36 Goryo-Ohara, Nishikyo-ku, Kyoto 615-8245, Japan
2. I Peace, Inc., 809 San Antonio Rd., Suite 7, Palo Alto, CA 94303, USA
3. Department of General Medicine, Faculty of Medicine, Juntendo University, Tokyo, Japan
4. Department of Tourism Medicine, Hyogo Medical University, Nishinomiya, Hyogo, Japan
5. KOSÉ Corporation, Tokyo, Japan

*Corresponding author: Koji Tanabe (tanabe@ipeaceinc.com)

Abstract

Skin aging involves remodeling of the dermal extracellular matrix (ECM), associated with reductions in hyaluronic acid (HA) and collagens. Although stem cell-derived conditioned media have shown regenerative potential, their clinical translation is limited by donor variability and limited manufacturing standardization. We established an end-to-end Good Manufacturing Practices (GMP) manufacturing and quality assurance framework for iPSC Factor (iPSF), an iPSC-derived bioactive preparation. This framework includes GMP iPSC generation, cell banking with comprehensive safety testing, animal component-free manufacturing, and predefined final-product release testing. iPSF enhanced HA production in human dermal fibroblasts in a concentration-dependent manner across independent iPSC clones, accompanied by selective induction of hyaluronan synthase 2 (*HAS2*) expression. Pharmacological inhibition and phosphorylation analyses demonstrated that transforming growth factor beta (TGF-β)/Smad and p38 mitogen-activated protein kinase signaling were involved in iPSF-induced HA production. RNA-seq showed that iPSF upregulated ECM-related genes, including *COL6A1*, *COL6A2*, *COL7A1*, *FN1*, and *BGN*. *In vivo*, repeated subcutaneous administration of iPSF increased dermal HA staining in rats and was associated with improved wound closure in mice. Repeated intravenous administration showed no

systemic toxicity. This GMP-manufactured iPSF promoted HA synthesis and modulated ECM-related gene expression, supporting its development as a standardized cell-free platform for skin regeneration and regenerative medicine.

Keywords

iPSC Factor (iPSF), induced pluripotent stem cells (iPSCs), Hyaluronic acid (HA), Extracellular matrix (ECM) remodeling, GMP manufacturing, Skin regeneration / skin aging

Introduction

Skin aging is characterized by progressive remodeling of the dermal extracellular matrix (ECM), resulting in reduced skin elasticity, dryness, and wrinkle formation [1–3]. Hyaluronic acid (HA) and collagen are major structural components of the dermal ECM that maintain tissue hydration, elasticity, and mechanical integrity. Both HA and collagen levels decline with age, contributing to impaired skin function and appearance [4,5]. Therefore, restoring ECM homeostasis is an important therapeutic strategy to prevent or slow skin aging.

Among the three hyaluronan synthase isoforms (HAS1–3), HAS2 is mainly responsible for HA synthesis in dermal fibroblasts and is essential for maintaining dermal HA homeostasis [4,6]. Therefore, selective induction of HAS2, together with broader remodeling of the ECM gene expression program, may represent a promising strategy for skin rejuvenation.

Stem cell-derived conditioned media (SC-CM) have attracted increasing attention as cell-free regenerative products. Mesenchymal SC-CM (MSC-CM) has been extensively investigated because it contains diverse bioactive factors that can promote tissue repair and skin regeneration [7,8]. However, the composition and biological activity of MSC-CM can be affected by donor-dependent cellular characteristics, creating challenges in manufacturing reproducibility, lot-to-lot consistency, and comprehensive quality control [9].

Induced pluripotent stem cells (iPSCs) possess extensive proliferative capacity and are amenable to standardized manufacturing under good manufacturing practice (GMP) conditions [10]. They can also be used to establish hierarchical cell banking systems, including Seed Stock, Seed Bank, and Master Cell Bank (MCB), thereby providing a foundation for controlled manufacturing, traceability, and consistent product

72 quality. These features make iPSC-derived conditioned medium (iPSC-CM) an attractive
73 candidate for development as a standardized cell-free product.

74 The biological activity and safety of iPSC-CM depend on the final conditioned
75 medium (CM) as well as the quality of the originating donor cells, established iPSCs, cell
76 banks, and manufacturing process [11]. Accordingly, the potential risk of infectious agent
77 transmission should be carefully assessed and controlled throughout the production
78 process. These processes should also comply with regulatory requirements for human-
79 derived starting materials, including the Japanese Standards for Biological Ingredients
80 and, where applicable, donor eligibility requirements under 21 CFR Part 1271, Subpart C
81 [11,12].

82 Furthermore, in the present manufacturing process, iPSCs were generated and
83 maintained under a GMP-controlled quality system, which involved the following
84 aspects: (1) establishing and managing cell banks; (2) tracing from the donor and starting
85 cells through the established iPSC line, cell banks, raw materials, and manufacturing
86 processes to the final product lots; (3) controlling raw materials and manufacturing
87 processes; (4) characterizing the identity, undifferentiated state, genomic stability, and
88 other relevant attributes of the iPSC banks; (5) microbiological safety testing; and (6)
89 final-product quality testing and release based on predefined specifications. Despite the

90 importance of these manufacturing and quality assurance considerations, few studies have
91 comprehensively evaluated unfractionated iPSC-CM by integrating biological
92 characterization with a controlled manufacturing and quality assurance framework.

93 iPSC-CM has been reported to exert beneficial effects in a range of tissue models,
94 including cardiac, corneal, kidney, and lung models, through mechanisms such as
95 suppression of apoptosis, oxidative stress, inflammation, and fibrosis, as well as
96 promotion of cell proliferation [13–18]. However, studies specifically examining its
97 effects on dermal fibroblasts remain comparatively limited. Previous studies
98 demonstrated that iPSC-CM promotes the proliferation and migration of human dermal
99 fibroblasts [19], whereas iPSC-derived extracellular vesicles and microvesicles restore
100 collagen expression in aged or UV-damaged fibroblasts [20,21]. However, most studies
101 have focused on extracellular vesicle fractions rather than unfractionated conditioned
102 medium. Consequently, it remains unclear whether unfractionated iPSC-CM promotes
103 HA synthesis and modulates the coordinated expression of ECM-related genes. The
104 intracellular signaling mechanisms underlying these biological effects are also poorly
105 understood.

106 In this study, we established an end-to-end GMP manufacturing and quality
107 assurance workflow for iPSC Factor (iPSF), a cell-free iPSC-derived bioactive

preparation, and investigated its effects on dermal ECM-associated processes. Using *in vitro* models, we evaluated iPSF's effects on HA synthesis, ECM-related gene expression, and the molecular mechanisms underlying its biological activity. We further assessed iPSF efficacy in rat skin and murine wound-healing models, and its systemic safety after repeated intravenous administration to support its translational potential. Our findings demonstrate that iPSF is a promising standardized cell-free therapeutic platform for skin regeneration with potential for future regenerative medicine applications.

Results

Establishment of a GMP manufacturing and quality-control workflow for iPSF

We established a standardized end-to-end GMP manufacturing and quality-control workflow for producing iPSC Factor (iPSF), a proprietary iPSC-derived bioactive preparation generated through a controlled iPSC culture and collection process. This workflow includes donor qualification, non-integrating iPSC generation, hierarchical cell banking, expansion of production iPSCs, controlled collection and filtration, and final-product release testing (Figure 1A).

Because the manufacturing platform was designed to support allogeneic applications, we assessed donor eligibility before blood collection and iPSC induction by

126 reviewing relevant medical history and communicable-disease risk factors, and testing
127 donor blood samples for predefined blood-borne and other relevant communicable
128 disease agents. These processes were performed in compliance with donor-eligibility
129 requirements, including 21 CFR Part 1271, Subpart C. Testing was performed in
130 laboratories certified under the Clinical Laboratory Improvement Amendments of 1988
131 (CLIA), using appropriate FDA-licensed, approved, or cleared donor-screening assays,
132 including nucleic acid-, antigen-, and/or antibody-based assays, following the
133 manufacturers' instructions. Based on the screening and testing results, the donor met all
134 predefined eligibility criteria and was deemed eligible. Peripheral blood mononuclear
135 cells (PBMCs) derived from this donor were subsequently reprogrammed using a non-
136 integrating method. We then established a three-tier cell-banking system consisting of
137 Seed Stock, Seed Bank, and MCB.

138 As shown in Figure 1A, quality-control testing was conducted at predefined
139 stages of cell-line establishment and cell banking, with test panels selected according to
140 the purpose and status of each stage. Across the Seed Stock, Seed Bank, and MCB stages,
141 the iPSCs were evaluated, as applicable, for cell identity, pluripotency, viability,
142 karyotypic integrity, residual reprogramming vectors, sterility, mycoplasma, endotoxin,
143 and human viral safety. Genomic quality was assessed at the Seed Bank and MCB stages

using next-generation sequencing (NGS)-based cancer gene panel analysis. Only cell lines meeting all predefined acceptance criteria were advanced for manufacturing. At the MCB stage, comprehensive GMP-compliant viral safety testing was performed in accordance with applicable regulatory requirements and guidance, including *in vitro* and *in vivo* adventitious virus assays, retrovirus testing, transmission electron microscopy (TEM), and targeted testing for relevant human viruses.

Qualified MCB-derived iPSCs were expanded under standard culture conditions. Before collecting CM for iPSF production, the culture medium was replaced with Puel, a proprietary animal-origin-free medium developed by I Peace, Inc. for culturing and maintaining human iPSCs. To verify that Puel supports the maintenance of essential iPSC characteristics, the morphology, proliferative capacity, and pluripotency marker expression of human iPSCs cultured in Puel were evaluated. These cells exhibited typical compact colony morphology, and their growth kinetics were comparable to those observed in the conventional Essential 8 (E8) medium during serial passaging (Supplementary Figure S1A, B). Flow cytometric analysis showed that 98.2% of cells were positive for pluripotency-associated markers TRA-1-60 and SSEA-4. Immunofluorescence (IF) staining confirmed robust expression of another set of pluripotency-associated markers, OCT3/4 and LIN28A (Supplementary Figure S1C, D).

These findings indicate that Puel supports the maintenance and expansion of undifferentiated human iPSCs, validating its use as a culture medium for iPSF production. The CM was collected under controlled GMP conditions and clarified by filtration. The resulting iPSF lots were released only after fulfilling predefined specifications for sterility, mycoplasma, endotoxin, and relevant human viral pathogens. Together, these procedures established a standardized GMP manufacturing pipeline, from donor qualification and iPSC generation to cell banking, conditioned-medium production, and final-product release.

iPSF promotes HA production along with *HAS2* induction

To determine whether iPSF promotes HA production, human dermal fibroblasts (HDFs) were treated with increasing concentrations of iPSF, and the HA released into the culture medium was quantified. HA production increased progressively in cells treated with up to 80% (v/v) iPSF but declined at 100% (Figure 1B). Importantly, even at concentrations as low as 1%, we observed a substantial increase in HA production in independent experiments examining the lower concentration range (Supplementary Figure S2A). We observed that HDF cell numbers were markedly reduced under the 100% iPSF condition (Supplementary Figure S2B), which most likely explains the lower HA level.

To explore the molecular mechanism underlying increased HA production, we analyzed hyaluronan synthase gene expression by qPCR. iPSF treatment significantly increased *HAS2* expression, whereas that of *HAS3* was not significantly changed (Figure 1C). *HAS1* transcripts were below the detection limit in both control and iPSF-treated HDFs. Consistent with these findings, IF analysis confirmed that increased *HAS2* expression was accompanied by enhanced HA accumulation following iPSF treatment (Figure 1D).

To further characterize the HA-promoting activity of iPSF, we compared its effect with that of CM prepared from differentiated iPSCs. CM from differentiated iPSCs exhibited a significantly weaker effect on HA production than iPSF (Figure 1E), indicating that the HA-promoting activity present in iPSF is markedly reduced in this CM.

To assess whether the HA-promoting activity of iPSF is reproducible across independent iPSC clones, iPSF preparations generated from two iPSC clones were evaluated, and their CM preparations were compared with those from adipose-derived mesenchymal stromal cells (AD-MSCs) and human amniotic mesenchymal stromal cells (HA-MSCs). Both iPSF preparations exhibited significantly higher HA levels compared with the control (Figure 1F). Notably, although the two MSC-derived CM also demonstrated significantly increased HA production, the HA production observed for

198 both iPSF preparations was significantly higher than that of these CM preparations under
199 the experimental condition (Figure 1F). In a separate experiment, CM prepared from
200 Muse cells also induced *HAS2* expression; however, the magnitude of induction was
201 lower than that observed with iPSF under the conditions tested (Figure 1G).

202 Because iPSF may contain both iPSC-conditioned medium and components
203 released from disrupted iPSCs, we next examined whether an iPSC extract alone could
204 induce *HAS2* expression. The iPSC extract increased *HAS2* expression (Figure 1H),
205 suggesting that intracellular iPSC-derived components may contribute to the activity of
206 iPSF. These findings indicate that HAS2-inducing activity is present not only in iPSF but
207 also in the iPSC extract. Collectively, these findings show that iPSF robustly promotes
208 HA production and HAS2 expression, with greater activity than MSC- or Muse-derived
209 conditioned media under the conditions tested. The activity of iPSC extracts further
210 suggests that intracellular iPSC-derived components contribute to the biological activity
211 of iPSF.

212

213 **TGF-β/Smad and p38 MAPK signaling contribute to iPSF-induced HA production**

214 To investigate the signaling pathways underlying the iPSF-induced increase in HA
215 production, HDFs were treated with inhibitors targeting the Bone Morphogenetic Protein

(BMP), Transforming Growth Factor beta (TGF-β) receptor, and p38 Mitogen-Activated Protein Kinase (MAPK) pathways. In the absence of inhibitors, iPSF markedly increased HA production compared with the control (Figure 2A). The TGF-β receptor pathway inhibitor SB431542 significantly attenuated iPSF's stimulatory effect on HA production. Another TGF-β receptor inhibitor, RepSox, produced a similar but comparatively weaker reduction. Inhibition of p38 MAPK signaling with BIRB796 also significantly suppressed iPSF-induced HA production. In contrast, the BMP pathway inhibitors dorsomorphin or DMH1 had no significant effect on the response, suggesting that this pathway plays a limited role under these conditions.

To determine whether iPSF activates these signaling pathways, phosphorylation of Smad2/3 and p38 MAPK was evaluated by IF staining. iPSF-treated HDFs exhibited increased phospho-Smad2/3 and phospho-p38 signals compared with control cells (Figure 2B and D), as shown using quantitative analysis (Figure 2C and E). Collectively, these findings indicate that TGF-β/Smad and p38 MAPK signaling contribute to the HA-promoting effects of iPSF in HDFs.

iPSF promotes transcriptional remodeling of extracellular matrix-associated genes

To comprehensively evaluate iPSF-induced transcriptional changes, we performed RNA sequencing using HDFs. Among 12,946 genes analyzed, 1,246 genes were differentially expressed (adjusted $p < 0.05$ and |log2 fold change| > 1), including 734 upregulated and 512 downregulated genes (Figure 3A; Supplementary Data S1).

Among the upregulated genes, several ECM-related genes, including *HAS2*, *COL6A1*, *COL6A2*, and *COL7A1*, were prominent. Furthermore, genes involved in cell adhesion and ECM organization, including *DST*, *PLEC*, *BGN*, and *FN1*, were also upregulated (Figure 3A and C).

To assess the biological significance of these transcriptional changes, Gene Ontology (GO) analysis was performed using the upregulated genes. Significant enrichment of ECM-related cellular components, including collagen-containing extracellular matrix, hemidesmosome, and filopodium membrane, was observed (Figure 3B). Collectively, these findings indicate that iPSF promotes a broad transcriptional program associated with ECM formation and cell adhesion, extending beyond the induction of *HAS2* alone.

In vitro and _in vivo_ validation of the extracellular matrix–promoting effects of iPSF

To determine whether the biological activities of iPSF observed *in vitro* translate into tissue-level regenerative effects *in vivo*, we first evaluated its effects on dermal HA deposition in rats following repeated local administration. Twelve-month-old Sprague–Dawley rats received daily subcutaneous injections of iPSF or phosphate-buffered saline (PBS) into paired dorsal skin sites for 14 consecutive days (Figure 4A). Immunohistochemical analysis revealed stronger HA staining in the superficial dermis of iPSF-treated skin than in paired PBS-treated skin (Figure 4B), consistent with the enhanced HA production observed in cultured fibroblasts.

Because re-epithelialization requires coordinated keratinocyte migration during wound repair, we next examined whether iPSF directly promotes keratinocyte migration using an Oris stopper-based cell migration assay. iPSF significantly enhanced keratinocyte migration in a concentration-dependent manner, with the greatest effect observed at 10% iPSF (Figure 4C, D).

Finally, to determine whether these effects are associated with improved wound repair, we evaluated iPSF in a murine full-thickness excisional wound model (Figure 4E). Representative photographs demonstrated greater wound closure in iPSF-treated wounds than in PBS-treated controls on day 11 (Figure 4F).

Taken together, these findings indicate that iPSF enhances dermal HA deposition, promotes keratinocyte migration, and potentially improves wound closure, supporting its regenerative potential in skin tissue.

Safety evaluation of repeated intravenous administration of iPSF in rats

To evaluate the systemic safety of iPSF, Sprague–Dawley rats received daily intravenous injections of iPSF (5 g/kg/day) or vehicle for 14 consecutive days, followed by necropsy on Day 15 (Figure 5A). No mortality or treatment-related clinical signs were observed. Body weight increased steadily in both male and female animals during the treatment period, with no apparent differences between the control and iPSF-treated groups (Figure 5B).

Organ weights were comparable between the control and iPSF-treated groups (Figure 5C). Serum biochemical, hematological, and coagulation parameters also showed no consistent treatment-related changes (Figure 5D–F). Minor differences were observed in several individual parameters; however, these changes were limited in magnitude, occurred only in one sex, and were not accompanied by any histopathological abnormalities. Therefore, they were considered incidental rather than toxicologically relevant. Complete datasets are provided in Supplementary Table S4. Histopathological

examination of major organs and tissues, including the brain, heart, liver, kidney, lung, spleen, reproductive organs, and skin, revealed no changes following repeated iPSF administration. Figure 5G summarizes the tissues examined and the related findings. Collectively, repeated intravenous administration of iPSF at 5 g/kg/day for 14 days was well tolerated in rats, with no evidence of systemic toxicity under the test conditions.

Discussion

This study establishes an end-to-end GMP manufacturing and quality assurance framework for iPSC Factor (iPSF), an iPSC-derived bioactive preparation with promising translation potential.

Although the regenerative properties of stem cell-derived CM and secretome-related products have been widely investigated, the manufacturing and quality control processes for these complex biological preparations for clinical translation remain understudied. Beyond biological activity, the cellular starting material, donor qualification, cell banking strategy, genomic and microbiological characteristics, manufacturing process, traceability, and final-product release criteria of a stem-cell-derived product must be defined and controlled before human use. In this study, these elements were integrated into a unified manufacturing framework extending from donor

qualification and iPSC establishment through hierarchical cell banking, production, and final iPSF release. This approach links the quality of the cellular source and manufacturing process with the biological properties of the final product. The use of iPSCs offers several advantages over primary differentiated cells, including mesenchymal stromal/stem cells (MSCs), which have finite replicative capacity and progressively undergo replicative senescence and phenotypic changes during prolonged culture [22]. Moreover, MSCs derived from bone marrow, adipose tissue, umbilical cord, and other tissues represent biologically distinct populations that may differ in transcriptional profiles, proliferative properties, surface-marker expression, and secretory activity [9,23]. Consequently, products manufactured using primary cells may be influenced by donor-to-donor and tissue-to-tissue variability and may ultimately require new donors or new source-cell lots as replicative capacity becomes limiting. In contrast, iPSCs possess extensive self-renewal capacity and can support repeated manufacturing cycles from the same qualified MCB. Their identity and state can also be defined using predefined quality attributes, including pluripotency, morphology, genomic integrity, and microbiological safety. Although biological variability among iPSC lines cannot be completely eliminated, manufacturing from a stable and extensively characterized cell bank may provide a more reproducible and controllable cellular starting material for long-term production.

Another distinction between iPSCs and primary-cell sources is the cells' biological age. Because primary cells retain characteristics influenced by the donor's chronological age, physiological history, and environmental exposures, cellular aging may affect their proliferative capacity, secretory phenotype, and biological activity. Reprogramming to pluripotency, in contrast, resets multiple age-associated cellular features, including epigenetic state, telomere biology [24,25] , mitochondrial function, and senescence-associated phenotypes [26] . Thus, although donor-derived genetic variation and acquired mutations might remain, iPSC-based manufacturing may partially decouple the biological state of the production cell from the chronological age of the original donor. This property is particularly relevant for secretome-based products, in which age-associated changes in the source cells could influence the composition and activity of the preparation.

Other adult stem-cell populations have also been explored as regenerative cell sources. For example, Muse (multilineage-differentiating stress-enduring) cells are characterized as a stage-specific embryonic antigen 3 (SSEA-3)-positive subpopulation within mesenchymal cell populations and possess several properties relevant for regenerative medicine [27]. However, they represent a relatively limited population within adult tissues and have more restricted proliferative capacity than iPSCs, making

their isolation, enrichment, and maintenance during extended expansion challenging. In contrast, iPSCs can be clonally established, extensively characterized, banked, and expanded while maintaining a defined pluripotent state. These differences may become particularly important when the objective is not transplantation of the cells themselves, but reproducible large-scale manufacture of bioactive preparations derived from them.

Another advantage of an iPSC-based production platform is its scalability. iPSCs are amenable to three-dimensional suspension or aggregate culture, enabling substantially higher cell densities per unit culture volume than conventional adherent primary-cell systems [28]. Because the amount of cell-derived biological material available for collection may depend on the number and metabolic or secretory activity of the production cells, high-density culture facilitates production of desired amounts of concentrated iPSC-derived bioactive preparations while reducing culture volume and manufacturing footprint. However, cell density alone does not necessarily predict biological potency, and future process development should systematically define the relationships among culture density, cellular state, product composition, and biological activity.

Beyond these manufacturing considerations, this study provides mechanistic evidence for iPSF's biological activity. iPSF increased HA production in HDFs, and this

357 effect was associated with increased *HAS2* expression, whereas *HAS3* expression was not
358 significantly altered. Pharmacological inhibition of TGF-β receptor signaling or p38
359 MAPK significantly attenuated iPSF-induced HA production, and iPSF treatment
360 increased phosphorylation of Smad2/3 and p38. Collectively, these findings support that
361 the TGF-β/Smad and p38 MAPK signaling pathways might be involved in the HA-
362 promoting activity of iPSF. This is consistent with previous reports demonstrating that
363 TGF-β/Smad and p38 MAPK signaling can induce *HAS2* expression in dermal fibroblasts
364 [29,30]. However, because inhibition of either pathway did not completely abolish the
365 response, a single signaling pathway is unlikely to explain the observed biological effect.
366 The molecular constituents within a complex iPSC-derived bioactive preparation
367 remain underexplored. iPSF may contain multiple classes of biologically active
368 constituents, such as proteins, peptides, extracellular vesicle-associated components,
369 metabolites, and other cell-derived molecules. Therefore, iPSF's biological activity may
370 result from the integrated effects of multiple components acting independently or
371 cooperatively through different cellular pathways, rather than from a single dominant
372 factor. This possibility is consistent with the RNA-seq findings, which showed that the
373 response to iPSF extended beyond *HAS2* and involved coordinated changes in multiple
374 ECM-associated genes, including *COL6A1*, *COL6A2*, *COL7A1*, *FN1*, *BGN*, *DST*, and

375 *PLEC* [31–35]. Thus, iPSF might modulate a broader ECM-associated transcriptional
376 program rather than acting exclusively on HA synthesis. Future studies combining
377 biochemical fractionation, proteomic and metabolomic profiling, extracellular-vesicle
378 analysis, and functional screening will help identify the principal bioactive constituents
379 and determine whether biological activity depends on individual molecules, their
380 combinations, or interactions among different classes of components. Such studies may
381 also facilitate the development of mechanism-relevant potency assays that more directly
382 link critical product attributes with biological activity.

383 Although this study focused primarily on dermal fibroblasts and skin-related
384 biological responses, iPSF activity may not be restricted to HA production or to a single
385 cell type. In addition to increasing *HAS2* expression and HA synthesis, iPSF altered the
386 expression of multiple ECM-associated genes and promoted keratinocyte migration.
387 These results suggest that iPSF may influence broader cellular functions related to tissue
388 homeostasis, ECM organization, cell migration, and repair, warranting further systematic
389 evaluation of its role in inducing related or distinct biological responses in other relevant
390 cell types and tissues, such as keratinocytes, vascular endothelial cells, immune cells,
391 muscle cells, and neuronal cells. This may help distinguish shared biological activities
392 from cell type-specific responses and clarify the broader biological scope of iPSF. Such

studies may also reveal potential applications of iPSF beyond skin regeneration and provide insights into the cellular programs modulated by this iPSC-derived bioactive preparation.

Preliminary *in vivo* observations further supported the cellular and transcriptional findings. Repeated local administration of iPSF increased dermal HA staining in rats, suggesting that the HA-promoting activity observed in cultured fibroblasts can also occur within intact skin tissue. iPSF also promoted keratinocyte migration *in vitro*, consistent with qualitative evidence of improved wound closure observed in the murine wound model. These findings highlight a broader regenerative effect involving ECM-associated responses and cellular processes relevant to tissue repair. Nevertheless, the magnitude, reproducibility, and durability of these effects should be validated using quantitative wound-healing analyses, histological assessment, and evaluation in additional animal models.

Several important translational parameters should be defined before clinical application in humans. The biologically effective exposure of iPSF in human tissues is currently unknown. The optimal dose, formulation, administration route, treatment frequency, and duration may vary by intended indication. Intradermal or subcutaneous administration may provide relatively high local exposure for skin-directed applications,

411 whereas topical, systemic, or other delivery approaches may require different formulation,
412 distribution, and pharmacokinetic considerations. Future studies should define the
413 relationships among administered dose, local tissue exposure, pharmacodynamic
414 responses such as HA induction, and the duration of biological activity. The minimum
415 biologically effective dose and the exposure-response relationship should be established
416 to define clinically relevant dosing regimens.

417 Another important consideration before human application is the cellular origin
418 of iPSF. Allogeneic manufacture offers substantial practical advantages because a single
419 qualified iPSC bank can facilitate standardized large-scale manufacturing and the
420 availability of an off-the-shelf product. Nevertheless, such preparations may contain
421 donor-derived proteins, extracellular vesicles, or other biological constituents that could
422 potentially elicit immune responses, particularly with repeated or long-term
423 administration. Allogeneic production also requires rigorous donor qualification and
424 testing to minimize the potential transmission of communicable agents. Therefore,
425 autologous iPSF generated from an individual's own qualified iPSC line represents an
426 alternative strategy that warrants further investigation, particularly for repeated or long-
427 term treatment. This approach could reduce exposure to unrelated donor-derived
428 biological constituents and avoid transmission of infectious agents originating from an

unrelated donor. However, risks associated with adventitious contamination or infectious agents already present in the individual cannot be eliminated, requiring additional considerations related to manufacturing time, cost, and individualized quality control. Therefore, a direct comparison of autologous and allogeneic iPSF will help determine the optimal manufacturing and treatment strategy for different clinical applications.

We initially assessed the systemic tolerability of the iPSF formulation using a repeated-dose intravenous study. Daily intravenous administration of iPSF at 5 g/kg/day for 14 days resulted in no mortality, clinical abnormalities, consistent hematological or biochemical changes, organ-weight alterations, or histopathological findings. Importantly, this study was designed primarily to assess systemic tolerability under a high-exposure condition rather than a clinically relevant therapeutic dose. Therefore, the absence of detectable systemic toxicity should be interpreted as initial safety information, and not as the human dosing range. Longer-term repeated-exposure studies, immunological assessments, and route-specific toxicology will be required to establish intended clinical applications and dosing regimens.

Several limitations of this study should be acknowledged. The principal bioactive constituents responsible for iPSF activity and signaling mechanisms beyond TGF-β/Smad and p38 MAPK remain poorly defined. The ECM-associated transcriptional

447 changes identified by RNA-seq were not comprehensively validated at the protein or
448 tissue-structural level. Furthermore, HA was evaluated primarily by total abundance
449 rather than by molecular-weight distribution, which may influence biological activity [36].
450 The number of independent iPSC lines examined was limited, and additional lines
451 representing broader donor backgrounds are needed to further establish biological and
452 manufacturing reproducibility. The biological effects of iPSF were evaluated primarily in
453 skin-related cell types and tissues, necessitating further investigations in other cell
454 populations. *In vivo* efficacy was also evaluated in a limited number of models, and
455 clinically relevant dosing and administration regimens remain to be established. Finally,
456 the immunological, manufacturing, and practical differences between autologous and
457 allogeneic iPSF will require direct experimental and clinical evaluation.

458 In conclusion, this study establishes an integrated GMP manufacturing and
459 quality assurance framework for iPSF. The prepared iPSC-derived bioactive formulation
460 promoted HA synthesis in association with *HAS2* induction, at least in part through TGF-
461 β/Smad and p38 MAPK signaling, while also modulating a broader ECM-associated
462 transcriptional program. This platform enables manufacture from a qualified, renewable
463 iPSC source with improved scalability of iPSC culture and the potential to reduce
464 variability associated with donor, tissue origin, cellular senescence, and donor age,

providing a rationale for using iPSCs as a source of bioactive regenerative preparations. Together with the preliminary *in vivo* efficacy and systemic safety findings, these results facilitate further development of iPSF as a standardized cell-free regenerative platform. Future studies should aim to identify the bioactive constituents, characterize effects across different cell types and tissues, establish mechanism-relevant potency assays and human dosing parameters, and evaluate autologous and allogeneic manufacturing strategies to facilitate clinical translation.

Methods

Ethical approval and informed consent

Human induced pluripotent stem cells (iPSCs) used in this study were established by I Peace, Inc. from peripheral blood mononuclear cells (PBMCs) obtained from a human donor. The procedures involving human donor-derived samples for iPSC generation in this study were reviewed and approved by WCG IRB (Institutional Review Board; affiliated with WCG Clinical, Inc., USA; WIRB IPCE-TA001; Protocol No. 20202719). The approved procedures included donor recruitment, medical screening, blood collection, iPSC generation, and storage, together with the associated informed consent procedures.

Written informed consent was obtained from the donor prior to blood collection and iPSC generation, including consent for the subsequent research use of the derived iPSCs. All procedures were conducted in accordance with the relevant ethical guidelines and regulations and the IRB-approved protocol.

The human dermal fibroblast line ASF-4-6 used in this study belongs to the ASF-4 series, a collection of fibroblast lines established from skin tissue collected from the same donor, Dr. Kazuhiko Kaji, at different ages over several decades. The establishment and characterization of the ASF-4 series have been previously described [37], and cells from this series, including ASF-4-1 and ASF-4-6, have also been used in a subsequent study by Itai et al. [38]. The ASF-4-6 cells used in the present study were kindly provided by Dr. Kaji.

The research project entitled "Involvement of Cellular Senescence in Human Aging" was reviewed and approved by the Ethics Committee of Nihon Pharmaceutical University on February 15, 2016 (Document No. Nichiyakurin 27-04). Dr. Kaji himself was both the tissue donor and the principal investigator of the approved research project. As explicitly stated in the original ethics application, a formal informed consent procedure was not conducted because the tissue donor was the investigator himself. The application disclosed these circumstances and included the planned establishment and research use

of ASF-4-6. The Ethics Committee subsequently determined that the research proposal complied with the university's ethical regulations. All procedures were conducted in accordance with the relevant institutional ethical guidelines and regulations.

ASF-4-1 through ASF-4-5 have been registered in the Japanese Collection of Research Bioresources (JCRB) Cell Bank. ASF-4-6 has also been submitted to the JCRB Cell Bank for deposition and is currently undergoing quality control testing prior to public availability.

Other commercially available human cells were purchased from Thermo Fisher Scientific, ScienCell Research Laboratories, ATOM Stem Cells, and Kurabo Industries, as described in the relevant Methods sections.

Donor eligibility assessment

Donor eligibility was assessed based on medical history, communicable-disease risk assessment, and laboratory testing for predefined blood-borne and other relevant communicable disease agents, based on the donor-screening principles described in 21 CFR Part 1271, Subpart C. Laboratory testing was performed by CLIA-certified laboratories using appropriate donor-screening assays, including FDA-licensed, approved,

518 or cleared assays where applicable. Only cells obtained from donors who met the
519 predefined eligibility criteria were used for subsequent iPSC generation.
520
521 **GMP-controlled manufacturing and qualification of iPSCs**
522 Human induced pluripotent stem cells (iPSCs) were generated from donor-derived
523 peripheral blood mononuclear cells (PBMCs) under GMP-controlled conditions
524 according to a previously described reprogramming procedure [39]. Briefly, OCT3/4,
525 SOX2, KLF4, and L-MYC were introduced into PBMCs using a non-integrating Sendai
526 virus-based GMP CytoTune reprogramming system (ID Pharma Co., Ltd., Japan).
527 Following reprogramming, emerging iPSC colonies were selected, established, and
528 expanded in StemFit^{TM} Basic03 (GMP) medium (Ajinomoto Co., Inc., Japan).
529 Established iPSC lines were maintained and sequentially expanded in StemFit^{TM}
530 Basic03 (GMP) medium to establish a Seed Stock (P6), Seed Bank (P8), and Master Cell
531 Bank (MCB; P11). Stage-specific quality-control testing was performed during cell-bank
532 establishment according to the testing scheme (Figure 1A). Quality-control testing
533 followed the predefined requirements for each banking stage. Seed Stock testing included
534 residual Sendai virus (SeV) reprogramming vector, sterility, and endotoxin. Seed Bank
535 testing included sterility, mycoplasma, endotoxin, a human viral panel, cell identity by

536 short tandem repeat (STR) profiling, pluripotency assessment by flow cytometric analysis
537 of TRA-1-60 and SSEA-4 expression, post-thaw viability, karyotype analysis, and a
538 targeted next-generation sequencing-based cancer-associated gene panel.

539 The quality and safety of the MCB were evaluated comprehensively before
540 release for subsequent use. This involved extensive viral safety characterization,
541 including a predefined human viral panel, *in vitro* and *in vivo* adventitious-agent assays,
542 retrovirus detection by fluorescent product-enhanced reverse transcriptase (F-PERT)
543 assay, transmission electron microscopy (TEM), and residual SeV vector testing.
544 Additional MCB release tests included sterility, mycoplasma, endotoxin, cell identity by
545 STR profiling, pluripotency assessment by flow cytometric analysis of TRA-1-60 and
546 SSEA-4 expression, post-thaw viability, karyotype analysis, and the targeted cancer-
547 associated gene panel.

548 Only MCBs that met all predefined quality and acceptance criteria were used for
549 subsequent iPSC-CM manufacturing.

550

551 **GMP-controlled manufacturing of iPSC Factor (iPSF)**

552 For iPSF production, MCB-derived iPSCs were thawed and seeded at 5×10^4 cells/well
553 in one well of a six-well plate coated with iMatrix-511MG. Cells were cultured in

554 StemFit™ Basic03 (GMP) medium supplemented with Y-27632CS. The medium was
555 first changed two days after seeding and every two days thereafter. After colony
556 expansion, cells were detached using CTS™ Versene (EDTA) and passaged at 8×10^4
557 cells/dish onto three 90-mm dishes coated with iMatrix-511MG. Cells were cultured in
558 StemFit™ Basic03 (GMP) medium supplemented with Y-27632CS. The medium was
559 changed two days after passaging and seeding and every two days thereafter. After further
560 expansion, cells were detached again using CTS™ Versene (EDTA) and passaged at $8 \times$
561 10^4 cells/dish onto 70 iMatrix-511MG-coated 90-mm dishes. Cells were cultured in the
562 same medium, and the medium was changed two days after passaging and every two days
563 thereafter. When the cultures reached approximately 50–60% confluence, the medium
564 was replaced with Puel medium (I Peace, Inc.), an animal-origin-free medium
565 manufactured in a GMP-controlled environment for iPSF production.

566 On day 7 after seeding, the cells reached approximately 80% confluence, and the
567 culture supernatant was collected, centrifuged at 200 ×g for 5 min to remove residual
568 intact cells and larger cellular debris, and then passed through a 0.22-μm filter. The filtrate
569 was designated iPSC Factor (iPSF), aliquoted into serum tubes at 2 mL/tube, and
570 promptly stored at −80°C until further use.

As shown in Figure 1A, predefined release testing was performed on the iPSCs collected from the culture supernatant and the final product, iPSF. For the iPSCs, post-thaw cell count and viability were assessed, together with pluripotency marker expression by immunocytochemical staining for OCT3/4 and LIN28A and flow cytometric analysis of TRA-1-60 and SSEA-4. iPSF was tested for sterility, mycoplasma, endotoxin, and a predefined panel of relevant human viral pathogens. iPSF that met all predefined release specifications was stored at −80°C until use.

Culture of human dermal fibroblasts

HDFs were cultured in fibroblast medium, comprising high-glucose DMEM supplemented with 10% fetal bovine serum (FBS) and antibiotic-antimycotic (Thermo Fisher Scientific). The following fibroblast lines were used: ASF-4-6 (previously described [37,38]), and commercially available adult HDFs (Thermo Fisher Scientific, C0135C).

Preparation of MSC-conditioned medium

Human adipose-derived mesenchymal stromal cells (AD-MSCs; ScienCell, Cat. No. 7510) and amniotic mesenchymal stromal cells (HA-MSCs; ScienCell, Cat. No. 7140)

were cultured in Mesenchymal Stem Cell (MSC) medium (ScienCell, Cat. No. 7501) according to the manufacturer's instructions. Cells were seeded at 2×10^6 cells/10-cm dish. After two days, the medium was replaced with fresh MSC medium, and conditioned medium (CM) was collected after an additional two days of incubation. The collected CM was centrifuged at 200 ×g for 5 min to remove cellular debris and subsequently passed through a 0.22-μm filter. The resulting MSC-CM was used in Figure 1F.

Preparation of Muse cell-conditioned medium

Human umbilical cord-derived Muse cells (ATOM MUSE [SSEC™], ATOM Stem Cells, USA) were seeded at a density of 2.5×10^5 cells per 6-cm dish in medium comprising high-glucose DMEM supplemented with 15% FBS and antibiotic-antimycotic (Thermo Fisher Scientific). Two days after seeding, the culture medium was replaced with fresh 15% FBS DMEM medium. On day 4, the medium was replaced with 10 mL of Puel medium. After an additional 2 days of culture, the conditioned medium was collected and passed through a 0.22-μm filter. The resulting filtrate was designated as Muse cell-conditioned medium (Muse-CM) and used for subsequent experiments.

Preparation of differentiated iPSC-conditioned medium

Human iPSCs were dissociated and transferred to ultra-low attachment culture dishes for suspension culture in human ES medium for seven days to generate embryoid bodies (EBs). The EBs were subsequently plated onto tissue culture dishes and cultured in DMEM supplemented with 10% FBS for seven days to allow spontaneous outgrowth and differentiation. The outgrown cells were then dissociated with 0.05% trypsin–EDTA, replated onto new tissue culture dishes, and cultured in DMEM containing 10% FBS for a week.

When the differentiated cells reached approximately 70%–80% confluence, the culture medium was replaced with serum-free DMEM and incubated for 48 h. The CM was then collected, centrifuged at 200 ×g for 5 min to remove cellular debris, and passed through a 0.22-μm filter. This clarified supernatant was used as differentiated iPSC-CM in subsequent experiments.

Preparation of iPSC extract

Human iPSCs (1×10^7 cells) were suspended in 5 mL of fibroblast medium and stored at −80°C for 24 h. The frozen cell suspension was then thawed at room temperature and centrifuged at 200 × g for 5 min to remove cellular debris. The resulting supernatant was passed through a 0.22-μm filter, and the filtrate was designated as 100% iPSC extract.

For subsequent experiments, the iPSC extract was diluted to the indicated concentrations (v/v) with fibroblast medium. 40% iPSC extract and 80% iPSF were used for the experiment shown in Figure 1H.

Assessment of iPSC proliferation

To compare the proliferative capacity of iPSCs under different culture conditions, iPSCs were seeded at 1×10^4 cells/well in six-well plates and cultured in either Essential 8 (E8) medium or Puel (I Peace, Inc.). Cells were cultured for five days before each passage, dissociated into single cells, and reseeded at the same density (1×10^4 cells/well) for subsequent passages. At each passage, viable cells were manually counted using a hemocytometer, and their numbers were presented on a $\log_{10}$ scale.

Hyaluronic acid Enzyme-Linked Immunosorbent Assay (ELISA)

HDFs were seeded at 1×10^5 cells/well in six-well plates and cultured in fibroblast medium. The following day, the culture medium was replaced with fibroblast medium containing the indicated concentrations of iPSF. iPSF was diluted with fibroblast medium. After two days, culture supernatants were collected and diluted as appropriate. HA

concentrations were measured using a Hyaluronan Quantikine ELISA Kit (R&D Systems, Cat. No. DHYAL0) according to the manufacturer's instructions.

Quantitative PCR (qPCR)

HDFs were seeded at 1×10^5 cells/well in six-well plates and cultured in fibroblast medium. The following day, the medium was replaced with iPSF-containing medium, and cells were treated for 48 h. Control cells were cultured in fibroblast medium without iPSF. Total RNA was extracted from cells using the NucleoSpin RNA Plus kit (MACHEREY-NAGEL) according to the manufacturer's instructions. cDNA was synthesized using ReverTra Ace qPCR RT Master Mix (TOYOBO). qPCR was performed using THUNDERBIRD Next SYBR qPCR Mix (TOYOBO) on a QuantStudio 3 system (Thermo Fisher Scientific). Primer sequences used are listed in Supplementary Table S1. GAPDH was used as the internal reference gene. Relative gene expression was calculated using the $2^{-\Delta\Delta Ct}$ method, normalized to GAPDH and expressed relative to the control group, which was set to 1 [40] .

Inhibitor screening assay for HA production

HDFs were seeded at 1×10^5 cells/well in six-well plates and allowed to attach overnight. The next day, cells were treated with iPSF or control medium in the presence of vehicle (DMSO) or the following signaling pathway inhibitors: dorsomorphin (0.5 μM; Selleck Chemicals, S7840) and DMH1 (0.5 μM; Selleck Chemicals, S7146) as BMP pathway inhibitors; RepSox (10 μM; Selleck Chemicals, S7233) and SB431542 (10 μM; Fujifilm, 033-24631) as TGF-β pathway inhibitors; and BIRB796 (2 μM; Selleck Chemicals, S1574) as a p38 MAPK inhibitor. Inhibitors (or DMSO) were added together with iPSF and maintained throughout the treatment period. After 48 h, culture supernatants were collected and centrifuged. HA concentrations were measured using a Hyaluronan Quantikine ELISA Kit (R&D Systems) according to the manufacturer's instructions. Values were normalized to the iPSF + DMSO condition within each experiment (set to 1).

Immunostaining

Cells were cultured on 12-well plates and treated as indicated. Treated cells were washed once with PBS, fixed with 4% paraformaldehyde for 15 min at room temperature, and washed with PBS. Finally, the cells were permeabilized and blocked with PBS containing 0.1% Triton X-100 and 5% calf serum for 30 min at room temperature.

Then, cells were incubated with primary antibodies diluted in permeabilization/blocking buffer for 60 min at room temperature. After washing with PBS, cells were incubated with Alexa Fluor–conjugated secondary antibodies for 30 min at room temperature in the dark. Nuclei were then counterstained with Hoechst 33258 (0.1 μg/mL; Cellstain Hoechst 33258 solution, Dojindo, H341) for 15 min at room temperature in the dark. After washing twice with PBS, the cells were maintained in PBS for imaging. Images were acquired using a fluorescence microscope under identical acquisition settings for all experimental conditions. Antibodies used in this study are listed in the Supplementary Table S2.

Quantification of immunostaining data

We analyzed fluorescence images using a custom Python pipeline. First, nuclei were segmented from the Hoechst channel by Otsu's thresholding followed by removal of small objects. The resulting binary mask was used to label individual nuclei. For each labeled nucleus, the Cy5-channel signal was quantified by integrating pixel intensities within the nuclear region (integrated intensity). Background fluorescence was estimated from non-nuclear pixels (the inverse of the nuclear mask) in the same field of view, and the mean background intensity was calculated. Background-corrected nuclear signal was

obtained by subtracting (mean background intensity × nuclear area) from the integrated nuclear Cy5 intensity. The corrected signal was then normalized to nuclear area to yield the mean nuclear intensity (background-corrected intensity/area). All images were processed using identical parameters across experimental conditions.

RNA sequencing and differential expression analysis

HDFs (ASF-4-6) were treated with iPSF or fibroblast medium (control) for four days. Total RNA was extracted using the NucleoSpin RNA Plus kit (MACHEREY-NAGEL) according to the manufacturer's instructions. RNA quality and quantity were assessed by electrophoresis and fluorometric quantification, respectively. Strand-specific mRNA sequencing libraries were prepared with an average insert size of approximately 200 bp. Sequencing was performed on the Illumina NovaSeq X Plus platform to generate paired-end reads (2 × 150 bp), with an average sequencing depth of approximately 60 million reads/sample. Over 96% of sequenced bases achieved a quality score of Q30 or higher.

Transcript-level quantification was performed using Salmon (v1.10) [41] with quasi-mapping against the human reference transcriptome (GENCODE v49, GRCh38). Transcript abundance estimates were summarized to gene-level counts using the tximport package by summing estimated counts for transcripts corresponding to the same gene.

Gene annotation was based on GENCODE v49, and downstream analyses included only protein-coding genes.

Differential expression analysis was performed using DESeq2 (v1.46.0) in R (v4.4.1) [42] with the following design formula:

design = ~ *condition*

Three replicates were analyzed for each condition. Count data were normalized using the median-of-ratios method implemented in DESeq2. Statistical significance was assessed using the Wald test, followed by Benjamini–Hochberg correction for multiple testing. Genes with an adjusted p-value < 0.05 and an absolute log2 fold change > 1 were considered significantly differentially expressed. The complete results of the differential expression analysis are provided in Supplementary Data S1.

Gene Ontology (GO) enrichment analysis was performed using the Enrichr web server (https://maayanlab.cloud/Enrichr/) [43] using significantly upregulated genes as the input. Enriched GO Cellular Component terms were ranked based on adjusted p-values. To visualize representative genes, relative expression values were calculated by converting the DESeq2 log2 fold change values to linear fold changes (2^log2FoldChange), with the control group set to 1. Differential expression patterns were visualized using Volcano plots. The RNA sequencing data have been deposited in

the Gene Expression Omnibus under accession number GSE345931 (to be released upon publication).

Animal study and subcutaneous injections of iPSF

The study was performed at Cyagen. The rat skin study was approved by the Institutional Animal Care and Use Committee (IACUC) of Cyagen Biomodels (Guangzhou) Co., Ltd. (Approval No. GACU25-SY111) and conducted in accordance with the National Laboratory Animal Welfare Ethics guidelines and relevant institutional regulations.

Three twelve-month-old female Sprague–Dawley rats were used to evaluate the *in vivo* effects of iPSF on skin ECM composition. Animals were acclimated for one week before the treatment and housed individually under standard controlled conditions with free access to food and water.

For subcutaneous injections, the dorsal skin was shaved carefully without damaging the skin surface. Each rat received daily subcutaneous injections of iPSF and phosphate-buffered saline (PBS) as a control into paired dorsal skin sites for 14 consecutive days. iPSF was administered undiluted at 50 μL/injection site. Control sites received an equal volume of PBS. For anesthesia, a mixture of Zoletil 50 (5 mg/kg body weight; final concentration, 25 mg/mL) and xylazine hydrochloride (10 mg/kg body

749 weight; final concentration, 50 mg/mL) was administered intramuscularly at a total
750 volume of 0.02 mL/100 g body weight. On day 14, animals were euthanized by CO_2
751 inhalation at a displacement rate of 30–70% of the euthanasia chamber volume per minute.
752 Dorsal skin tissues were harvested from the injection sites and processed for paraffin
753 embedding and sectioning for subsequent histological and immunohistochemical
754 analyses.
755
756 **Immunohistochemistry**
757 Paraffin-embedded skin sections were deparaffinized, rehydrated, and subjected to
758 antigen retrieval using EDTA buffer. Endogenous peroxidase activity was blocked with
759 hydrogen peroxide, followed by blocking with normal serum. Sections were incubated
760 overnight at 4°C with primary antibodies against HA (GeneTex, GTX17370). After
761 washing, HRP-conjugated secondary antibodies were applied, and immunoreactivity was
762 visualized using 3,3'-diaminobenzidine (DAB). Nuclei were counterstained with
763 hematoxylin. Stained sections were scanned, and representative images were obtained for
764 each condition. Staining intensity was quantified using the respective image analysis
765 software. Data were analyzed by comparing iPSF-treated sites with paired PBS control
766 sites within the same animal.

Wound healing mouse model

The wound healing study was performed at Cyagen. The study was approved by the Institutional Animal Care and Use Committee (IACUC) of Cyagen Biomodels (Guangzhou) Co., Ltd. (Approval No. GACU26-SY008) and conducted in accordance with institutional guidelines and applicable regulations.

Female C57BL/6J mice (8–12 weeks old) were anesthetized by intraperitoneal injection of 1.25% tribromoethanol (12.5 mg/mL) at a dose of 250 mg/kg body weight. After removing the dorsal hair, two 6-mm full-thickness excisional wounds were created on the dorsum of each mouse. Each wound was secured with silicone splints (inner diameter, 8 mm; outer diameter, 12 mm) using cyanoacrylate adhesive and interrupted sutures to minimize wound contraction [44] . The wounds were covered with a transparent dressing (Tegaderm). PBS or undiluted iPSF (50 μL/wound) solutions were injected subcutaneously once daily for 11 consecutive days (Days 0–10). Each treatment consisted of four injections around the wound margin and one injection into the wound bed. Wounds were photographed on Days 0 and 11. On Day 11, mice were euthanized by CO_2 inhalation at a displacement rate of 30–70% of the euthanasia chamber volume per minute, and wound tissues were collected for histological evaluation.

785

786 **Keratinocyte migration assay**

787 For this experiment, iPSC-conditioned medium (iPSF) was prepared using a conventional
788 human embryonic stem (hES) cell medium (DMEM/F12 supplemented with KnockOut
789 Serum Replacement (KSR), L-glutamine, non-essential amino acids, 2-mercaptoethanol,
790 penicillin/streptomycin, and 4 ng/mL basic fibroblast growth factor). Normal human
791 epidermal keratinocytes (Kurabo, KK-4109) were maintained in HuMedia-KG2 (Kurabo)
792 at 37°C in a humidified atmosphere containing 5% CO_2. Before the migration assay, cells
793 were treated with 10 μg/mL mitomycin C for 2 h to inhibit cell proliferation. Cells were
794 then seeded at 4×10^4 cells/well into collagen-coated Oris Cell Migration Assay plates
795 (Platypus Technologies) and cultured for 24 h. After removing the stoppers, cells were
796 washed with PBS and incubated with iPSF at final concentrations of 0.1%, 1%, or 10%
797 (v/v) prepared in HuMedia-KG2 assay medium. For dilution, DMEM/F-12 was used.
798 After 23 h, cells were stained with calcein-AM. Cell migration into the central detection
799 zone was quantified by measuring fluorescence intensity using a microplate reader
800 (excitation, 485 nm; emission, 538 nm).

801

802 **Safety assessment in rats**

An exploratory safety study was conducted using six-week-old Sprague–Dawley rats at BoZo Research Center Inc. All procedures were approved by the Institutional Animal Care and Use Committee (IACUC) of BoZo Research Center Inc. (Approval No. T230078) and conducted in accordance with institutional guidelines. Rats were assigned to control and treatment groups (n = 3/sex/group). iPSF was administered intravenously via the tail vein at 5 g/kg once daily for 14 consecutive days. Animals were monitored daily for clinical signs, and body weight was recorded throughout the 14-day dosing period.

At the end of the observation period, animals were fasted overnight (approximately 16–21 h) and anesthetized with 3.0% isoflurane by inhalation for both induction and maintenance of anesthesia. Blood samples were collected from the abdominal aorta for hematological, serum chemistry, and coagulation analyses using automated clinical analyzers.

Following blood collection, animals were euthanized by exsanguination via the abdominal aorta under isoflurane anesthesia and subjected to complete necropsy. Major organs, including the brain, pituitary, thyroid, thymus, heart, lungs, liver, spleen, kidneys, adrenal glands, and reproductive organs, were collected and weighed. Representative tissues were fixed in 10% neutral buffered formalin, embedded in paraffin, sectioned, and

stained with hematoxylin and eosin. A qualified veterinary pathologist at BoZo Research Center Inc. performed histopathological evaluation in accordance with the study protocol. Findings were graded and compared between the control and iPSF-treated groups. All data are presented as mean ± standard deviation (SD).

Statistical analysis

Statistical analyses were performed using Microsoft Excel and Python. Data are presented as mean ± standard deviation (SD). Comparisons between two groups were performed using an unpaired or paired two-tailed Student's *t*-test, as appropriate. Comparisons among three or more groups were performed using one-way analysis of variance followed by Tukey's multiple-comparisons test. Differential gene expression (DEG) analysis was performed using DESeq2 as described above. Statistical significance was set at $p < 0.05$.

Data availability

The RNA-sequencing data generated in this study have been deposited in the Gene Expression Omnibus (GEO) under accession number GSE345931 (https://www.ncbi.nlm.nih.gov/geo/query/acc.cgi?acc=GSE345931). During peer review, the dataset can be accessed using the reviewer access token: yhktaccavhwjrwd. All other

data supporting the findings of this study are available within the article and its Supplementary Information files or from the corresponding author upon reasonable request.

Author contributions

R.S. conceived and designed the study, performed experiments, analyzed and interpreted the data, prepared the figures, and drafted the manuscript. K.S. performed experiments to evaluate Puel. E.T. performed experiments to examine the effect of iPSF on HA synthesis *in vitro*. R. M. analyzed the data of animal wound healing experiments. S.T. contributed to the development and evaluation of the GMP manufacturing, quality-control framework and drafted the manuscript. K.T. supervised the study, contributed to study design and interpretation of the data, and critically revised the manuscript. K.K. provided the ASF-4-6 human dermal fibroblast line, contributed to the scientific interpretation of the study, and critically reviewed the manuscript. All authors reviewed and approved the final manuscript.

Funding

This research received no specific grant from funding agencies in the public, commercial, or not-for-profit sectors.

Competing interests

R.S., K.S., R.M., E.T., S.T., and K.T. are employees of I Peace, Inc. or I Peace, Ltd., which develops and sells iPSC Factor (iPSF), the product investigated in this study. K.K. is an employee of KOSÉ Corporation.

References:

1. Zorina, A., Zorin, V., Kudlay, D. & Kopnin, P. Molecular Mechanisms of Changes in Homeostasis of the Dermal Extracellular Matrix: Both Involutional and Mediated by Ultraviolet Radiation. *Int. J. Mol. Sci.* **23**, 6655 (2022).
2. Yi, J. *et al.* Elastin-derived extracellular matrix fragments drive aging through innate immune activation. *Nat. Aging* **5**, 2380–2398 (2025).
3. McCabe, M. C. *et al.* Alterations in extracellular matrix composition during aging and photoaging of the skin. *Matrix Biol. Plus* **8**, 100041 (2020).
4. Chylińska, N. & Maciejczyk, M. Hyaluronic Acid and Skin: Its Role in Aging and Wound-Healing Processes. *Gels* **11**, 281 (2025).
5. Terazawa, S., Nakajima, H., Tobita, K. & Imokawa, G. The decreased secretion of hyaluronan by older human fibroblasts under physiological conditions is mainly associated with the down-regulated expression of hyaluronan synthases but not with the expression levels of hyaluronidases. *Cytotechnology* **67**, 609–620 (2015).
6. Nagaoka, A. *et al.* Regulation of Hyaluronan (HA) Metabolism Mediated by HYBID (Hyaluronan-binding Protein Involved in HA Depolymerization, KIAA1199) and HA synthases in growth factor-stimulated fibroblasts. *J. Biol. Chem.* **290**, 30910–30923 (2015).

7. Li, X., Zhang, D., Yu, Y., Wang, L. & Zhao, M. Umbilical cord-derived mesenchymal stem cell secretome promotes skin regeneration and rejuvenation: From mechanism to therapeutics. *Cell Prolif.* **57**, e13586 (2024).
8. Liu, C. *et al.* The conditioned medium from mesenchymal stromal cells pretreated with proinflammatory cytokines promote fibroblasts migration and activation. *PLoS One* **17**, e0265049 (2022).
9. Česnik, A. B. & Švajger, U. The issue of heterogeneity of MSC-based advanced therapy medicinal products–a review. *Front. Cell Dev. Biol.* **12**, 1400347 (2024).
10. Novoa, J. J. *et al.* Good Manufacturing Practice–compliant human induced pluripotent stem cells: from bench to putative clinical products. *Cytotherapy* **26**, 556–566 (2024).
11. Sullivan, S. *et al.* Quality control guidelines for clinical-grade human induced pluripotent stem cell lines. *Regenerative Med.* **13**, 859–866 (2018).
12. Fda, C. *Guidance for Industry: Eligibility Determination for Donors of Human Cells, Tissues, and Cellular and Tissue-Based Products (HCT/Ps)*. http://www.fda.gov/cber/guidelines.htm. (2007).
13. Guo, X. *et al.* Induced pluripotent stem cell-conditional medium inhibits H9C2 cardiomyocytes apoptosis via autophagy flux and Wnt/β-catenin pathway. *J. Cell. Mol. Med.* **23**, 4358–4374 (2019).
14. Liu, Q. *et al.* Characterization of the ipsc-derived conditioned medium that promotes the growth of bovine corneal endothelial cells. *PeerJ* **2019**, (2019).
15. Tarng, D. C., Tseng, W. C., Lee, P. Y., Chiou, S. H. & Hsieh, S. L. Induced pluripotent stem cell-derived conditioned medium attenuates acute kidney injury by downregulating the oxidative stress-related pathway in ischemia–reperfusion rats. *Cell Transplant.* **25**, 517–530 (2016).
16. Zhou, Y. *et al.* Induced pluripotent stem cell-conditioned medium suppresses pulmonary fibroblast-to-myofibroblast differentiation via the inhibition of TGF-β1/Smad pathway. *Int. J. Mol. Med.* **41**, 473–484 (2018).
17. Gazdhar, A. *et al.* The secretome of induced pluripotent stem cells reduces lung fibrosis in part by hepatocyte growth factor. *Stem Cell Res. Ther.* **5**, (2014).
18. Li, L.-F. *et al.* Improvement of ventilator-induced lung injury by IPS cell-derived conditioned medium via inhibition of PI3K/Akt pathway and IP-10-dependent paracrine regulation. *Biomaterials* **34**, 78–91 (2013).
19. Oh, M., Kim, Y. J., Son, Y. J., Yoo, H. S. & Park, J. H. Promotive effects of human induced pluripotent stem cell-conditioned medium on the proliferation

and migration of dermal fibroblasts. *Biotechnol. Bioprocess Eng.* **22**, 561–568 (2017).
20. Oh, M., Lee, J., Kim, Y. J., Rhee, W. J. & Park, J. H. Exosomes derived from human induced pluripotent stem cells ameliorate the aging of skin fibroblasts. *Int. J. Mol. Sci.* **19**, 1715 (2018).
21. Bakhshandeh, B. *et al.* Transcriptomic and in vivo approaches introduced human iPSC-derived microvesicles for skin rejuvenation. *Sci. Rep.* **13**, 9963 (2023).
22. Wagner, W. *et al.* Replicative senescence of mesenchymal stem cells: A continuous and organized process. *PLoS One* **3**, (2008).
23. Hodgson-Garms, M., Moore, M. J., Martino, M. M., Kelly, K. & Frith, J. E. Proteomic profiling of iPSC and tissue-derived MSC secretomes reveal a global signature of inflammatory licensing. *NPJ Regen. Med.* **10**, (2025).
24. Takahashi, K. *et al.* Induction of pluripotent stem cells from adult human fibroblasts by defined factors. *Cell* **131**, 861–72 (2007).
25. Marion, R. M. *et al.* Telomeres Acquire Embryonic Stem Cell Characteristics in Induced Pluripotent Stem Cells. *Cell Stem Cell* **4**, 141–154 (2009).
26. Lapasset, L. *et al.* Rejuvenating senescent and centenarian human cells by reprogramming through the pluripotent state. *Genes Dev.* **25**, 2248–2253 (2011).
27. Kuroda, Y. *et al.* Unique multipotent cells in adult human mesenchymal cell populations. *Proc. Natl. Acad. Sci. U. S. A.* **107**, 8639–43 (2010).
28. Lin, X. & Bui, T.-V.-A. cGMP-Compliant Large-Scale Manufacturing of Human Induced Pluripotent Stem Cells: Current Progress and Challenges. *Cytotherapy* 102815 (2026) doi:10.1016/j.jcyt.2026.102815.
29. Stuhlmeier, K. M. & Pollaschek, C. Differential Effect of Transforming Growth Factor β (TGF-β) on the Genes Encoding Hyaluronan Synthases and Utilization of the p38 MAPK Pathway in TGF-β-induced Hyaluronan Synthase 1 Activation. *Journal of Biological Chemistry* **279**, 8753–8760 (2004).
30. Schiller, M. *et al.* Increased cAMP levels modulate transforming growth factor-β/smad-induced expression of extracellular matrix components and other key fibroblast effector functions. *Journal of Biological Chemistry* **285**, 409–421 (2010).
31. Nastase, M. V., Young, M. F. & Schaefer, L. Biglycan: A Multivalent Proteoglycan Providing Structure and Signals. *J. Histochem. Cytochem.* **60**, 963–975 (2012).
32. Lenselink, E. A. Role of fibronectin in normal wound healing. *Int. Wound J.* **12**, 313–316 (2015).

33. Künzli, K., Favre, B., Chofflon, M. & Borradori, L. One gene but different proteins and diseases: The complexity of dystonin and bullous pemphigoid antigen 1. *Exp. Dermatol.* **25**, 10–16 (2016).
34. Theocharidis, G. *et al.* Type VI collagen regulates dermal matrix assembly and fibroblast motility. *Journal of Investigative Dermatology* **136**, 74–83 (2016).
35. Amano, S., Ogura, Y., Akutsu, N. & Nishiyama, T. Quantitative analysis of the synthesis and secretion of type VII collagen in cultured human dermal fibroblasts with a sensitive sandwich enzyme-linked immunoassay. *Exp. Dermatol.* **16**, 151–155 (2007).
36. Stern, R., Asari, A. A. & Sugahara, K. N. Hyaluronan fragments: An information-rich system. *Eur. J. Cell Biol.* **85**, 699–715 (2006).
37. Kaji, K. *et al.* Donor age reflects the replicative lifespan of human fibroblasts in culture. *Hum. Cell* **22**, 38–42 (2009).
38. Itai, E. *et al.* Single-cell analysis of human dermal fibroblasts isolated from a single male donor over 35 years. *Exp. Dermatol.* **32**, 1982–1995 (2023).
39. Ban, H. *et al.* Efficient generation of transgene-free human induced pluripotent stem cells (iPSCs) by temperature-sensitive Sendai virus vectors. *Proc. Natl. Acad. Sci. U. S. A.* **108**, 14234–14239 (2011).
40. Livak, K. J. & Schmittgen, T. D. Analysis of relative gene expression data using real-time quantitative PCR and the 2-ΔΔCT method. *Methods* **25**, 402–408 (2001).
41. Patro, R., Duggal, G., Love, M. I., Irizarry, R. A. & Kingsford, C. Salmon provides fast and bias-aware quantification of transcript expression. *Nat. Methods* **14**, 417–419 (2017).
42. Love, M. I., Huber, W. & Anders, S. Moderated estimation of fold change and dispersion for RNA-seq data with DESeq2. *Genome Biol.* **15**, 550 (2014).
43. Chen, E. Y. *et al.* Enrichr: Interactive and collaborative HTML5 gene list enrichment analysis tool. *BMC Bioinformatics* **14**, 128 (2013).
44. Galiano, R. D., Michaels, J., Dobryansky, M., Levine, J. P. & Gurtner, G. C. Quantitative and reproducible murine model of excisional wound healing. *Wound Repair Regen.* **12**, 485–492 (2004).

Figure legends

Figure 1. iPSF promotes HA production in dermal fibroblasts.

A. Schematic of the GMP-compliant manufacturing process for iPSF, including iPSC expansion, conditioned medium (CM) collection, clarification, and quality-control testing.

B. Representative experiment showing dose-dependent increase in HA production in human dermal fibroblasts (HDF) treated with increasing concentrations of iPSF.

C. mRNA expression profiles of *HAS2* and *HAS3* in HDF treated with iPSF, assessed by qPCR. *HAS1* was not detected in either condition. Data are shown as mean ± SD (n = 3). ***$p < 0.001$; ns, not significant.

D. Representative immunofluorescence images of HAS2 protein and HA in HDFs treated with iPSF or control medium. Scale bar: 100 μm.

E. Comparison of the effects of iPSF and CM derived from differentiated iPSCs on HA production in HDF. Data are presented as mean ± SD (n = 3). ***$p < 0.001$ vs differentiated iPSCs' CM.

F. HA production in HDFs treated with iPSF from two independent iPSC clones (CL1, CL2) and conditioned medium from adipose-derived MSCs (AD) or HA-MSCs (HA). Data are shown as mean ± SD (n = 3). ***$p < 0.001$

G. Comparison of *HAS2* expression in HDFs treated with iPSF or Muse cell-conditioned medium (Muse-CM). Data are shown as mean ± SD (n = 3). *$p < 0.05$, **$p < 0.01$, ***$p < 0.001$.

H. *HAS2* mRNA expression in HDFs treated with iPSF or iPSC extract, assessed by qPCR. Data are shown as mean ± SD (n = 3). *$p < 0.05$.

Figure 2. TGF-β/Smad and p38 MAPK signaling contribute to iPSF-induced HA production in dermal fibroblasts.

A. Effects of inhibitors for the BMP pathway (dorsomorphin, DMH1), TGF-β pathway (Repsox, SB431542), and p38 (BIRB796) on iPSF-induced HA production in HDF. HA concentration is normalized to iPSF + DMSO. Data are shown as mean ± SD (n = 3). *$p < 0.05$, ***$p < 0.001$.

B. Representative immunofluorescence images of phospho-Smad2/3 in HDFs treated with iPSF or control medium. Scale bar: 100 μm.

C. Quantification of phospho-Smad2/3 signal intensity. Data are shown as box plots. **$p < 0.01$. We analyzed a total of 175 cells (control) and 287 cells (iPSF) from three images.

D. Representative immunofluorescence images of phospho-p38 in HDF treated with iPSF or control medium. Scale bar: 100 μm.

E. Quantification of phospho-p38 signal intensity. Data are shown as box plots (n = 3). *$p < 0.05$. We analyzed a total of 184 cells (control) and 269 cells (iPSF) from three images.

Figure 3. Transcriptomic changes induced by iPSF treatment in HDF.

A. Volcano plot of differentially expressed genes (DEGs) in iPSF-treated vs. control HDFs. Upregulated genes ($log_2FC > 1$, adjusted $p < 0.05$; n = 734) and downregulated genes ($log_2FC < -1$, adjusted $p < 0.05$; n = 512) are shown in red and blue, respectively. Selected ECM-related genes are labeled.

B. Gene Ontology (GO) enrichment analysis of upregulated genes. The top 10 enriched cellular component categories are shown, ranked by $-log_{10}$(adjusted p-value). The dashed line indicates adjusted $p = 0.05$.

C. Fold changes of selected upregulated genes grouped by functional category. Control was set to 1. Statistical significance was determined by the DESeq2 Wald test with Benjamini–Hochberg correction. **$p < 0.01$, ***$p < 0.001$.

Figure 4. *In vitro and in vivo* validation of the extracellular matrix–promoting effects of iPSF.

A. Experimental design of the *in vivo* study. Twelve-month-old female Sprague–Dawley rats received daily subcutaneous injections of PBS or iPSF into paired dorsal skin sites for 14 consecutive days, followed by tissue collection for histological analysis.

B. Representative immunohistochemical images of hyaluronic acid (HA) staining in PBS- and iPSF-treated rat skin. Red arrowheads indicate HA-positive regions in the superficial dermis. Scale bars: 100 μm.

C. Representative fluorescence images of normal human epidermal keratinocyte migration assessed using an Oris stopper-based cell migration assay following treatment with basal medium or medium supplemented with specific iPSF concentrations (0.1%, 1%, and 10%).

D. Quantification of keratinocyte migration shown in (C). Cell migration into the central detection zone was quantified by calcein-AM fluorescence intensity. Data are presented as mean ± SD (n = 5). *$p < 0.05$, **$p < 0.01$, ***$p < 0.001$ versus the corresponding control.

E. Experimental design of the murine wound-healing model. Female C57BL/6J mice (8–12 weeks old) received two full-thickness dorsal skin wounds stabilized with silicone splints. PBS or iPSF was administered daily by subcutaneous injection.

F. Representative photographs of wounds immediately after surgery (day 0) and on day 11 following treatment with PBS or iPSF. Scale bars, 5 mm.

Figure 5. Repeated intravenous administration of iPSF demonstrates a favorable systemic safety profile in rats.

A. Experimental design of the repeated-dose toxicity study. Six-week-old Sprague–Dawley rats received daily intravenous injections of vehicle or iPSF (5 g/kg/day) for 14 consecutive days and were euthanized on Day 15.

B. Body weight changes during the treatment period.

C. Organ weights at necropsy.

D−F. Serum biochemical, hematological, and coagulation parameters, respectively.

G. Summary of histopathological findings in major organs and tissues from rats administered vehicle or iPSF (5 g/kg/day, i.v.) for 14 consecutive days. No treatment-related microscopic findings were observed in any of the tissues examined (n = 3 animals/sex/group).

Data are presented as mean ± SD (n = 3 animals/sex/group). Complete organ weight, hematological, serum biochemical, and coagulation data are provided in Supplementary Table S4. Abbreviations are listed in Supplementary Table S3.

Supplementary figures and table legends

Supplementary Figure S1. Characterization of human iPSCs cultured in the proprietary Puel medium used for iPSF manufacturing.

A. Representative phase-contrast image showing the typical morphology of an undifferentiated human iPSC colony. Scale bar: 100 μm.

B. Growth curves of human iPSCs cultured in Puel and Essential 8 (E8) medium during serial passaging. Cell numbers are presented on a $\log_{10}$ scale.

C. Flow cytometric analysis of the pluripotency-associated surface markers TRA-1-60 and SSEA-4 in cultured human iPSCs.

D. Immunofluorescence staining showing expression of the pluripotency-associated markers OCT3/4 and LIN28A in cultured human iPSCs. Nuclei were counterstained with Hoechst. Scale bars: 50 μm.

Supplementary Figure S2. Effects of iPSF concentration on HA production and HDF cell number.

A. HA production in HDF following treatment with low concentrations of iPSF. Data are shown as mean ± SD (n = 3). *$p < 0.05$ and ***$p < 0.001$ vs control.

B. Single experiment showing the number of HDF following treatment with increasing concentrations of iPSF.

Supplementary Table S1. Primer sequences used for qPCR.

Primer sequences used for quantitative PCR analysis in this study. Forward (Fw) and reverse (Rv) primer sequences are listed for each target gene.

Supplementary Table S2. Antibodies used in this study.

Primary and secondary antibodies used for immunofluorescence (IF), immunohistochemistry (IHC), immunocytochemistry (ICC), and flow cytometry analyses. Supplier information, catalog numbers, host species, clone names, and working dilutions are provided.

Supplementary Table S3. Abbreviations used in the supplementary tables and figures.

Definitions of abbreviations used in the supplementary tables and figures.

Supplementary Table S4. Complete toxicological evaluation following repeated intravenous administration of iPSF in rats.

Complete organ weight, hematological, serum biochemical, and coagulation data from Sprague–Dawley rats following daily intravenous administration of vehicle or iPSF (5 g/kg/day) for 14 consecutive days. Data are presented as mean ± SD (n = 3 animals/sex/group).

Supplementary Data S1. Complete differential expression analysis of RNA-seq.

Differential expression analysis of protein-coding genes between iPSF-treated and control fibroblasts performed using DESeq2. The dataset includes gene symbol, gene biotype, baseMean, log2 fold change, relative expression (2^log2FoldChange), standard error (lfcSE), Wald statistic, *p*-value, and adjusted *p*-value (Benjamini–Hochberg correction).

Figure 1

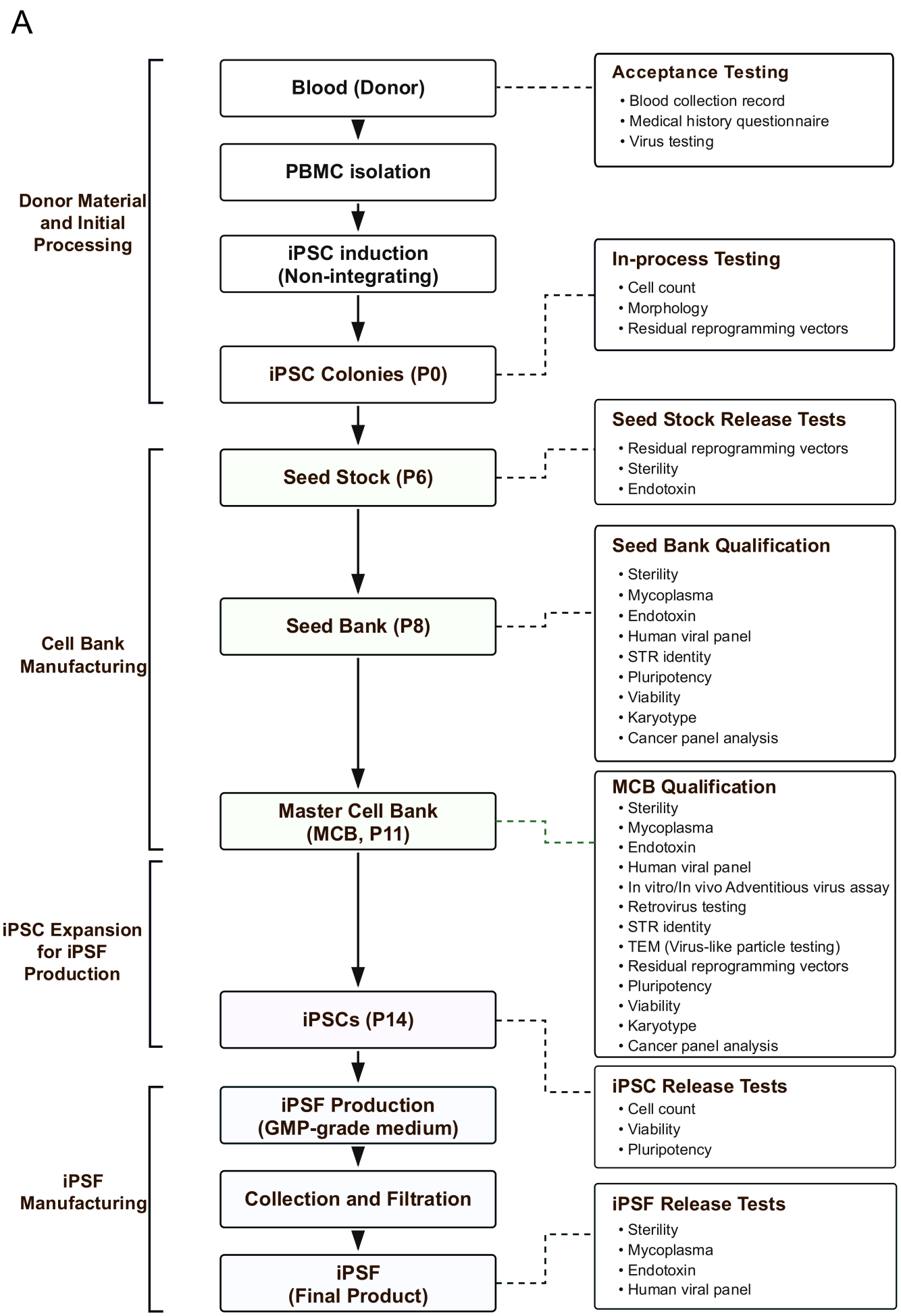
A
Donor Material and Initial Processing
Cell Bank Manufacturing
iPSC Expansion for iPSF Production
iPSF Manufacturing
Blood (Donor)
PBMC isolation
iPSC induction (Non-integrating)
iPSC Colonies (P0)
Seed Stock (P6)
Seed Bank (P8)
Master Cell Bank (MCB, P11)
iPSCs (P14)
iPSF Production (GMP-grade medium)
Collection and Filtration
iPSF (Final Product)
Acceptance Testing
• Blood collection record
• Medical history questionnaire
• Virus testing
In-process Testing
• Cell count
• Morphology
• Residual reprogramming vectors
Seed Stock Release Tests
• Residual reprogramming vectors
• Sterility
• Endotoxin
Seed Bank Qualification
• Sterility
• Mycoplasma
• Endotoxin
• Human viral panel
• STR identity
• Pluripotency
• Viability
• Karyotype
• Cancer panel analysis
MCB Qualification
• Sterility
• Mycoplasma
• Endotoxin
• Human viral panel
• In vitro/In vivo Adventitious virus assay
• Retrovirus testing
• STR identity
• TEM (Virus-like particle testing)
• Residual reprogramming vectors
• Pluripotency
• Viability
• Karyotype
• Cancer panel analysis
iPSC Release Tests
• Cell count
• Viability
• Pluripotency
iPSF Release Tests
• Sterility
• Mycoplasma
• Endotoxin
• Human viral panel

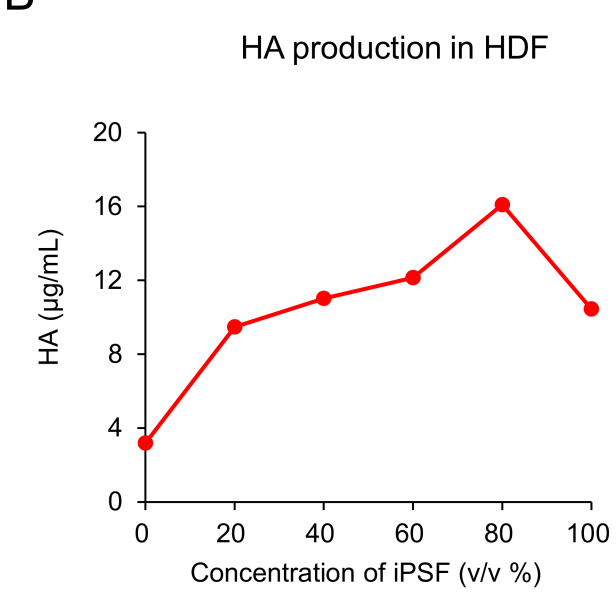
B
HA production in HDF
HA (μg/mL)
Concentration of iPSF (v/v %)
0
4
8
12
16
20
0
20
40
60
80
100

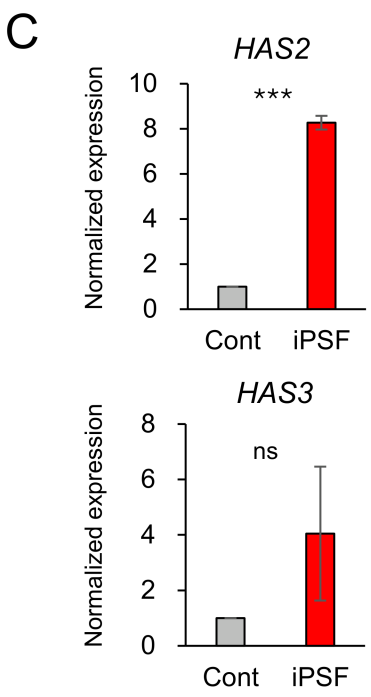
C
HAS2
Normalized expression
***
Cont
iPSF
HAS3
ns

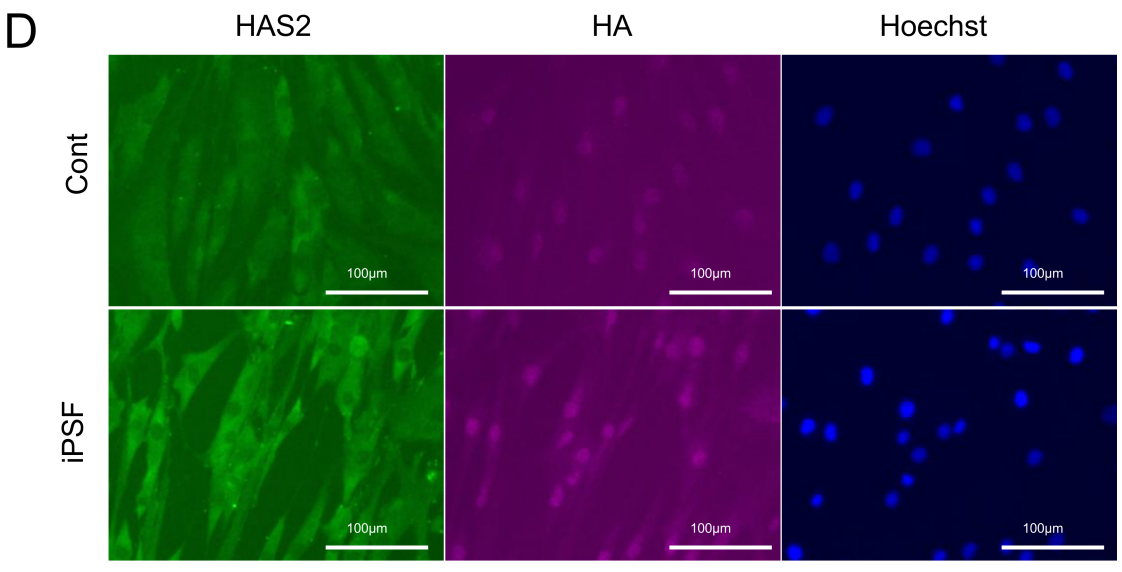
D
HAS2
HA
Hoechst
Cont
iPSF
100μm

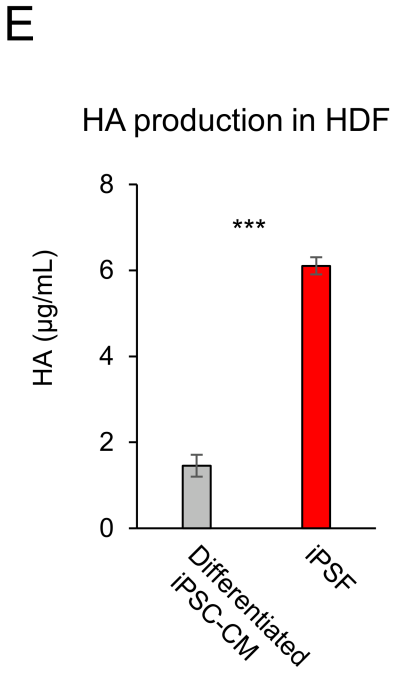
E
HA production in HDF
HA (μg/mL)
***
Differentiated iPSC-CM
iPSF

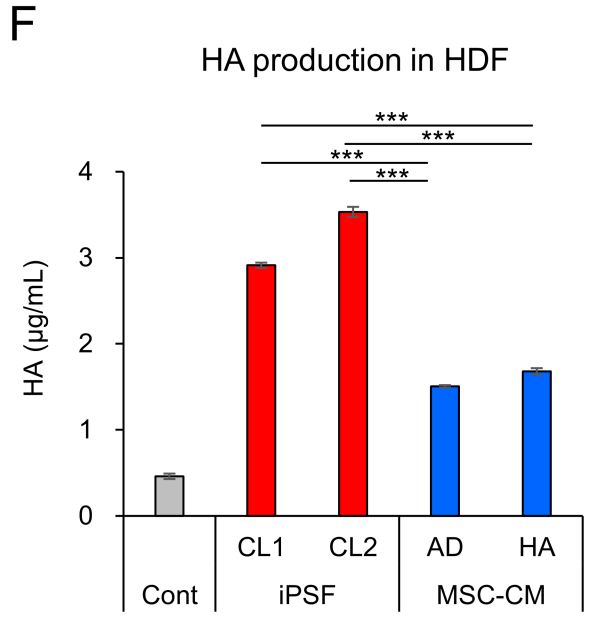
F
HA production in HDF
HA (μg/mL)
***
Cont
CL1
CL2
AD
HA
iPSF
MSC-CM

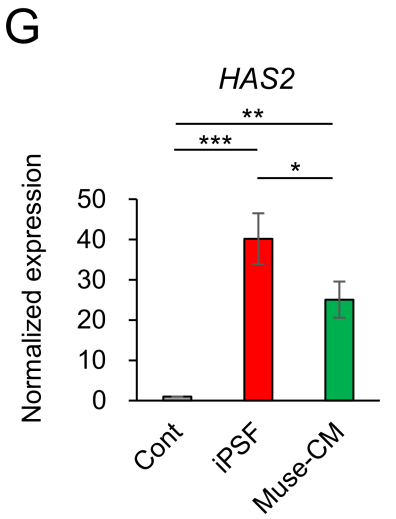
G
HAS2
Normalized expression
**
***
*
Cont
iPSF
Muse-CM

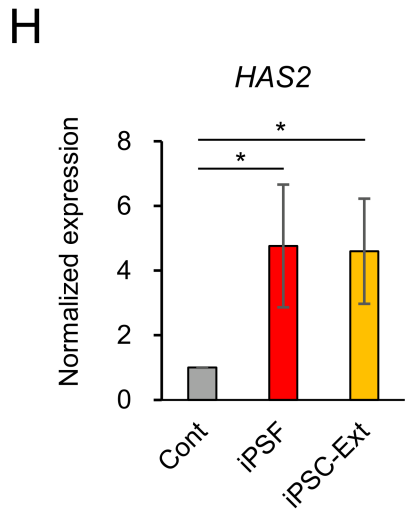
H
HAS2
Normalized expression
*
*
Cont
iPSF
iPSC-Ext

Figure 2

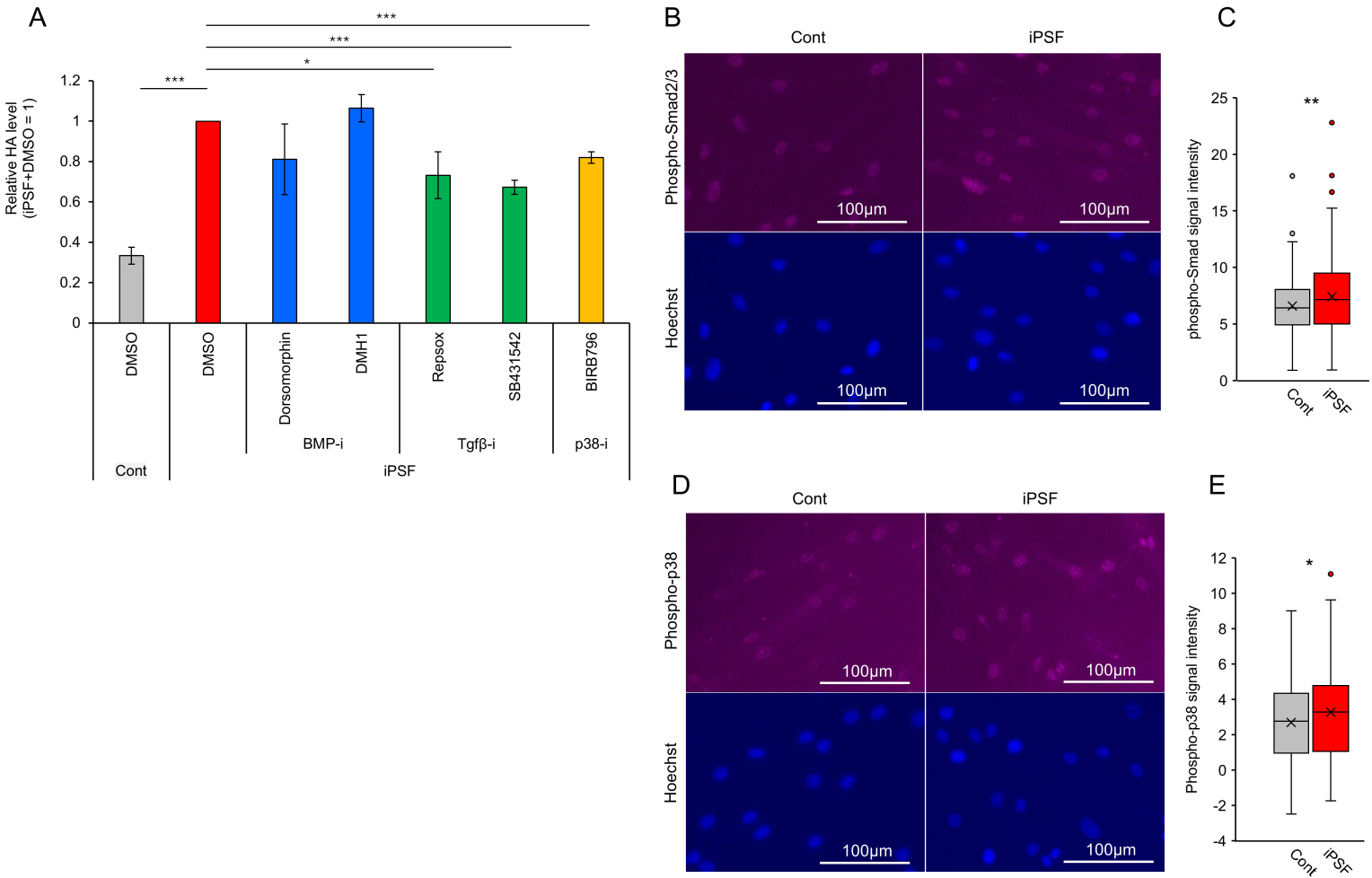
A
***
***
*
***
Relative HA level
(iPSF+DMSO = 1)
1.2
1
0.8
0.6
0.4
0.2
0
DMSO
DMSO
Dorsomorphin
DMH1
Repsox
SB431542
BIRB796
Cont
BMP-i
Tgfβ-i
p38-i
iPSF
B
Cont
iPSF
Phospho-Smad2/3
Hoechst
100μm
C
**
phospho-Smad signal intensity
25
20
15
10
5
0
Cont
iPSF
D
Cont
iPSF
Phospho-p38
Hoechst
100μm
E
*
Phospho-p38 signal intensity
12
10
8
6
4
2
0
-2
-4
Cont
iPSF

Figure 3

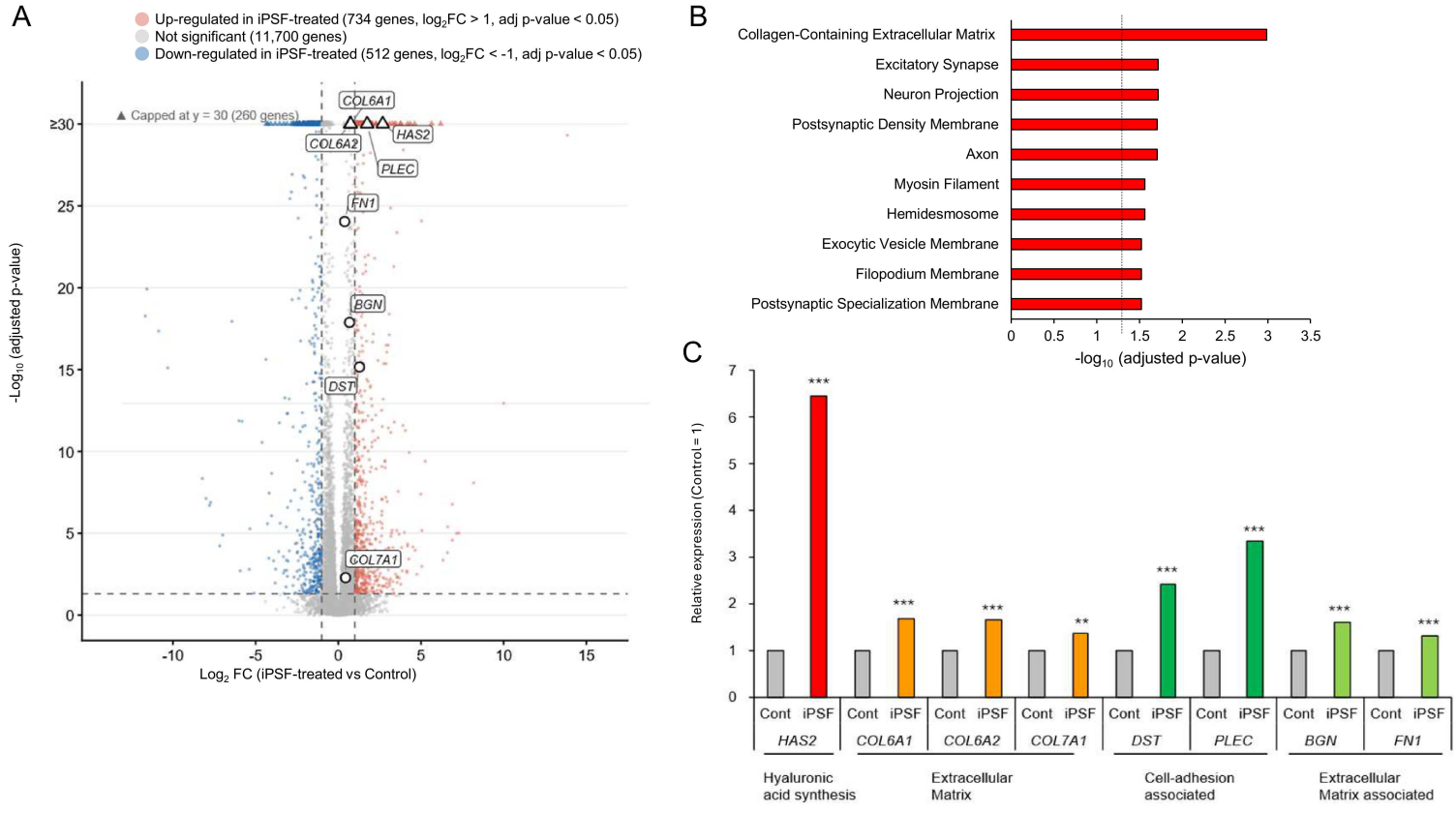
A
Up-regulated in iPSF-treated (734 genes, log2FC > 1, adj p-value < 0.05)
Not significant (11,700 genes)
Down-regulated in iPSF-treated (512 genes, log2FC < -1, adj p-value < 0.05)
▲ Capped at y = 30 (260 genes)
COL6A1
COL6A2
HAS2
PLEC
FN1
BGN
DST
COL7A1
-Log10 (adjusted p-value)
Log2 FC (iPSF-treated vs Control)
B
Collagen-Containing Extracellular Matrix
Excitatory Synapse
Neuron Projection
Postsynaptic Density Membrane
Axon
Myosin Filament
Hemidesmosome
Exocytic Vesicle Membrane
Filopodium Membrane
Postsynaptic Specialization Membrane
-log10 (adjusted p-value)
C
Relative expression (Control = 1)
Cont
iPSF
HAS2
COL6A1
COL6A2
COL7A1
DST
PLEC
BGN
FN1
Hyaluronic acid synthesis
Extracellular Matrix
Cell-adhesion associated
Extracellular Matrix associated

Figure 4

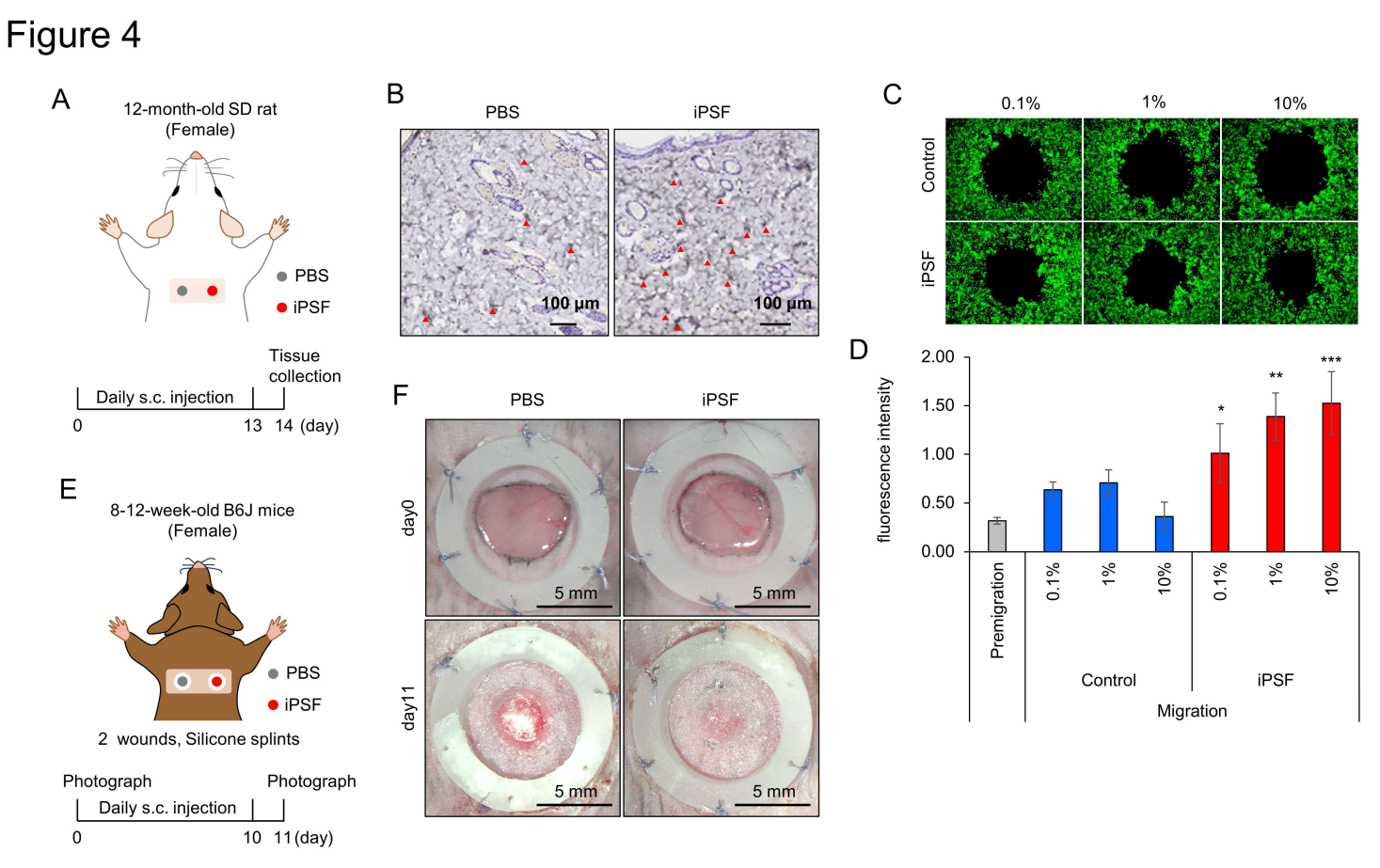
A
12-month-old SD rat
(Female)
PBS
iPSF
Tissue
collection
Daily s.c. injection
0
13
14 (day)
B
PBS
iPSF
100 μm
100 μm
C
0.1%
1%
10%
Control
iPSF
D
fluorescence intensity
2.00
1.50
1.00
0.50
0.00
*
**
***
Premigration
0.1%
1%
10%
0.1%
1%
10%
Control
iPSF
Migration
E
8-12-week-old B6J mice
(Female)
PBS
iPSF
2 wounds, Silicone splints
Photograph
Photograph
Daily s.c. injection
0
10
11 (day)
F
PBS
iPSF
day0
day11
5 mm
5 mm
5 mm
5 mm

Figure 5

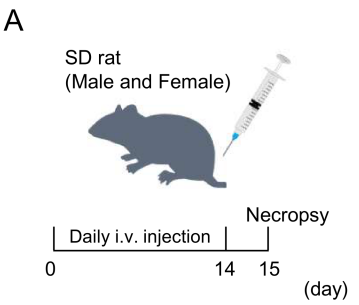

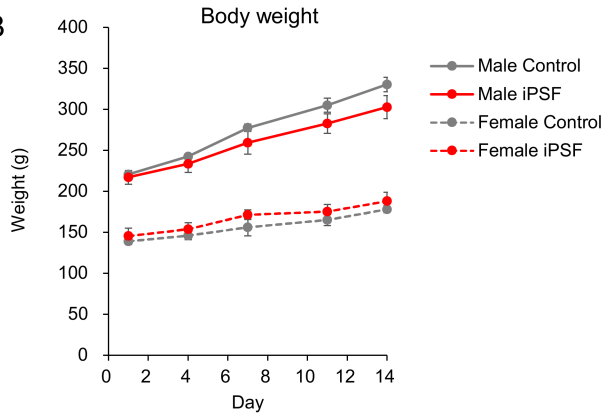

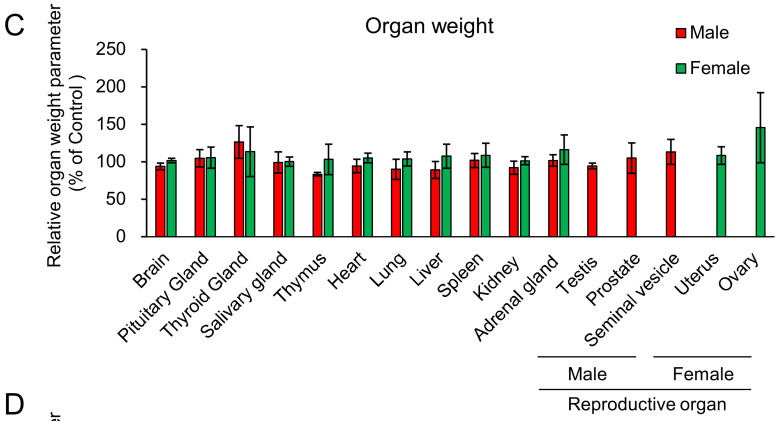

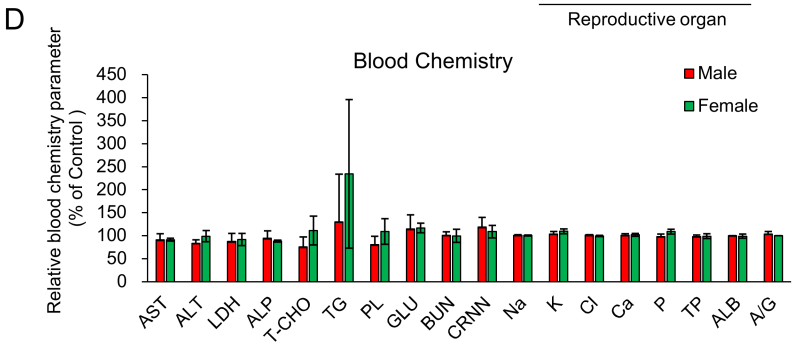

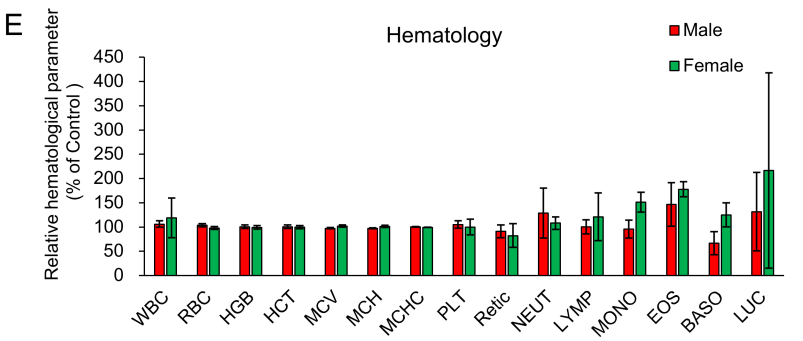

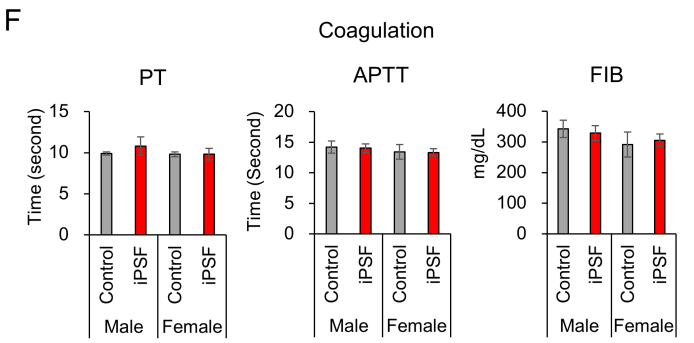

G

Organ/Tissue	Treatment-related finding
Brain	None
Spinal cord	None
Sciatic nerve	None
Optic nerve	None
Eye	None
Harderian gland	None
Pituitary gland	None
Thyroid gland	None
Parathyroid gland	None
Adrenal gland	None
Thymus	None
Spleen	None
Mandibular lymph node	None
Mesenteric lymph node	None
Peyer's patch	None
Heart	None
Aorta	None
Trachea	None
Lung	None
Tongue	None
Esophagus	None
Stomach	None
Duodenum	None
Jejunum	None
Ileum	None
Cecum	None
Colon	None
Rectum	None
Salivary gland	None
Liver	None
Pancreas	None
Kidney	None
Urinary bladder	None
Testis	None
Epididymis	None
Prostate	None
Seminal vesicle	None
Ovary	None
Uterus	None
Vagina	None
Mammary gland	None
Sternum	None
Femur	None
Bone marrow	None
Skeletal muscle	None
Skin	None

Supplementary Files

This is a list of supplementary files associated with this preprint. Click to download.

- SupplementaryTableS3Abbreviations.xlsx
- SupplementaryTableS4Toxicity.xlsx
- SupplementaryTableS2Antibodies.xlsx
- SupplementaryDataS1RNAseqDESeq2results.csv
- SupplementaryTableS1qPCRprimers.xlsx
- SupplementaryFigureS1.tif
- SupplementaryFigureS2.tif
- SupplementaryDataS1RNAseqDESeq2results.csv